

Digital Twin Generation from Visual Data: A Survey

Andrew Melnik, Benjamin Alt, Giang Nguyen, Artur Wilkowski, Maciej Stefańczyk, Qirui Wu, Sinan Harms, Helge Rhodin, Manolis Savva, and Michael Beetz

Abstract—This survey explores recent developments in generating digital twins from videos. Such digital twins can be used for robotics application, media content creation, or design and construction works. We analyze various approaches, including 3D Gaussian Splatting, generative in-painting, semantic segmentation, and foundation models highlighting their advantages and limitations. Additionally, we discuss challenges such as occlusions, lighting variations, and scalability, as well as potential future research directions. This survey aims to provide a comprehensive overview of state-of-the-art methodologies and their implications for real-world applications. Awesome list: <https://github.com/ndrwmlnk/awesome-digital-twins>

these 3D reconstructions and their associated processes using visual data, advancing from digital approximations to true Digital Twins. Recent advances in automatization of Digital Twin reconstruction from visual data provide opportunities for various domains, including robotics [2, 3], architecture, facility management, industrial fabrication, gaming, video stream compression, and virtual reality.

Traditionally, the creation of Digital Twins has relied on specialized hardware such as LiDAR scanners or hand-crafted CAD models. Recent advances in computer vision and machine learning, such as 3D Gaussian Splatting (3DGS), NeRF, and diffusion models, have opened new possibilities for simplifying this process using widely accessible video data. Videos, captured with ubiquitous devices such as smartphones, offer a rich source of spatial and visual information that can be leveraged for Digital Twins generation.

Another source of visual data is short videos generated by Video Diffusion Models (VDM) [4], which often suffer from a lack of physical plausibility. These limitations of VDMs can be mitigated by generating and animating Digital Twins based on the synthesized video content. Moving forward, the next frontier in 3D representation lies in enriching these DT models by integrating both the physical [5] and semantic [6] properties of objects.

Moreover, by analyzing demonstrations, such as a person interacting with a chest of drawers or a light switch, models can begin to absorb deeper contextual properties beyond mere geometry, like articulation of parts, hierarchical structure and connectivity, interaction properties, rules, associated processes, material properties, audio patterns, etc.

This survey focuses on the generation of Digital Twins (Figure 1) from images and videos, exploring the methods, challenges, and innovations that enable this transformative process. We aim to address key questions, including how to accurately reconstruct indoor environments, integrate semantic information, and ensure scalability across diverse use cases. The goal is to present approaches that not only enhance the fidelity of digital twins but also reduce the barriers to their adoption. We also highlight practical applications and outline future directions to advance the field further.



Fig. 1. Generating Indoor Digital Twins from Visual Data.

I. INTRODUCTION

DIGITAL Twins (DT)¹ are virtual representations of products, processes, and facilities that enterprises use to design, simulate, and operate their physical counterparts.

In the scope of this survey, we define Digital Twins as 3D models enriched with processes and semantic connections, similar to those in computer game environments and industrial CAD models. These models can range in accuracy from approximated 3D representations, like *Digital Cousins* [1] to highly detailed virtual replicas of real-world environments known as *Digital Twins*. Our focus will be on methodologies and understanding required to improve the accuracy of

Andrew Melnik, Benjamin Alt, Giang Nguyen, and Michael Beetz are with the University of Bremen, Germany

Artur Wilkowski, and Maciej Stefańczyk are with Warsaw University of Technology, Poland

Sinan Harms, and Helge Rhodin are with Bielefeld University, Germany

Qirui Wu, and Manolis Savva are with Simon Fraser University, Canada

Corresponding author: Andrew Melnik - andrew.melnik.papers@gmail.com

¹<https://www.nvidia.com/en-us/glossary/digital-twin/>

II. SHAPE RECONSTRUCTION

A. Mesh, CAD, 3DGS

Digital shape representations are usually based on mesh models, CAD models, and 3D Gaussian Splatting (3DGS) - each having distinct advantages. **Mesh** representation is

TABLE I
COMPARISON OF **3DGS**, **MESH**, AND **CAD** MODELS

Feature	3D Gaussian Splatting	Mesh Model	CAD Model
Representation	Gaussian splats (point-based with density, color, and opacity)	Polygonal (triangles/quads)	Mathematical (NURBS, B-Rep)
Precision	Approximate (view-dependent, continuous representation)	Approximate	Highly precise
Modifiability	Hard to modify (requires re-optimization)	Hard to modify	Easy to modify (parametric)
Usage	Real-time rendering, neural scene representation, volumetric rendering	3D graphics, gaming, animation, 3D printing	Engineering, manufacturing, design
File Size	Usually compact (but can grow with complexity)	Usually smaller	Larger due to parametric data
Rendering	Direct rendering via splatting (fast and efficient)	Rasterization or ray tracing	Mostly used for manufacturing, converted to mesh for visualization
Conversion	Difficult to convert to mesh or CAD	Can be converted to CAD (but loses precision)	Can be meshed or voxelized

using interconnected polygons (triangles or quads), making it efficient for real-time rendering, gaming, and 3D printing, though it lacks precise parametric control. **CAD** representation employs mathematical curves (NURBS, B-Rep) to create highly accurate, editable, and feature-based models, making it ideal for engineering, manufacturing, and design applications. **3D Gaussian Splatting** represents objects using point-based Gaussian functions with attributes like color, opacity, and density. This method excels in photorealistic, view-dependent rendering and is particularly useful for neural scene representations and volumetric graphics. Although **mesh** and **CAD** models are more structured and interpretable, **3DGS** offers a continuous and memory-efficient alternative for immersive applications (see Table I). The growing number of new methods for automated 3DGS reconstruction is establishing 3DGS as one of the key representations for approximating 3D scenes from visual input.

B. Video to intermediate 3D representations

a) COLMAP & Point Clouds: COLMAP [7] is a general-purpose Structure-from-Motion (SfM) pipeline. SfM [8], is a computer vision technique used to reconstruct a 3D representation of a scene from a set of 2D images taken from different viewpoints (Figure 2 b). The process involves detecting and matching features across images, reconstructing the motion of the camera, and using triangulation to recover the 3D structure of a scene [7]. The key part of SfM is determining both 3D geometry of the scene and the camera’s position and orientation relative to that geometry. SfM typically begins with feature detection, where key points such as edges, corners, and texture detected in each images using matching algorithms, ranging from classical techniques such as SIFT [9] to more recent deep learning-based approaches like SuperGlue [10], R2D2 [11], and LoFTR [12], which utilize neural networks or transformer architectures to achieve SOTA performance.

The corresponding features are then matched between the images, and by analyzing how key points move between the images, the algorithm determines the camera positions and orientations and camera intrinsic parameters. This allows for the reconstruction of 3D points using triangulation. To refine

the points and camera parameters, SfM uses bundle adjustments [13], reducing projection errors for higher accuracy. The result of this process is a sparse 3D point cloud. A point cloud is a collection of discrete points in 3D space that represents the surface geometry of an object or a scene. Each point has (X, Y, Z) coordinates, defining its position in space. Additional attributes such as color, intensity, and normal vectors can be stored with each point to enhance visualization and processing. These point clouds serve as the foundational data structure for many 3D modeling techniques, including mesh generation and virtual scene reconstruction. In some cases SfM is extended with Multi-View Stereo (MVS) to generate a dense point cloud that captures more details of the scene [14].

b) SLAM: Simultaneous Localization and Mapping is a fundamental concept in robotics and computer vision: estimating a camera’s motion in an unknown environment while building a 3D map of the surroundings. Previously SLAM systems used point clouds [20], surfels [21], or volumetric representations [22, 23, 24], relying on handcrafted feature tracking and pose estimation pipelines. While effective for basic localization, these systems struggle with photorealism, robustness in dynamic or low-texture environments. Recent advances introduce differentiable, learning-based representations, most notably 3D Gaussian Splatting [15], to address these limitations. Originally designed for novel view synthesis with known camera parameters, recent works [25, 26, 27] adapt 3DGS for SLAM by jointly optimizing camera poses and scene geometry via online tracking and incremental mapping. The differentiability of 3DGS enables gradient-based tracking using geometric (depth accuracy) and photometric (color consistency) loss functions over rendered and observed frames [25, 26, 27, 28, 29, 30, 31]. SLAM systems can also benefit from the compactness and continuity of Gaussian primitives improving the memory efficiency. Several works address this topic by compressing Gaussian attributes [32], reducing the number of Gaussian primitives by introducing opaque/transparent Gaussians [33], or introducing uncertainty-aware Gaussian fields to balance tracking robustness [34]. In terms of pose estimation, most systems assume a constant velocity or speed assumption [25, 26, 28]. Initial poses are then

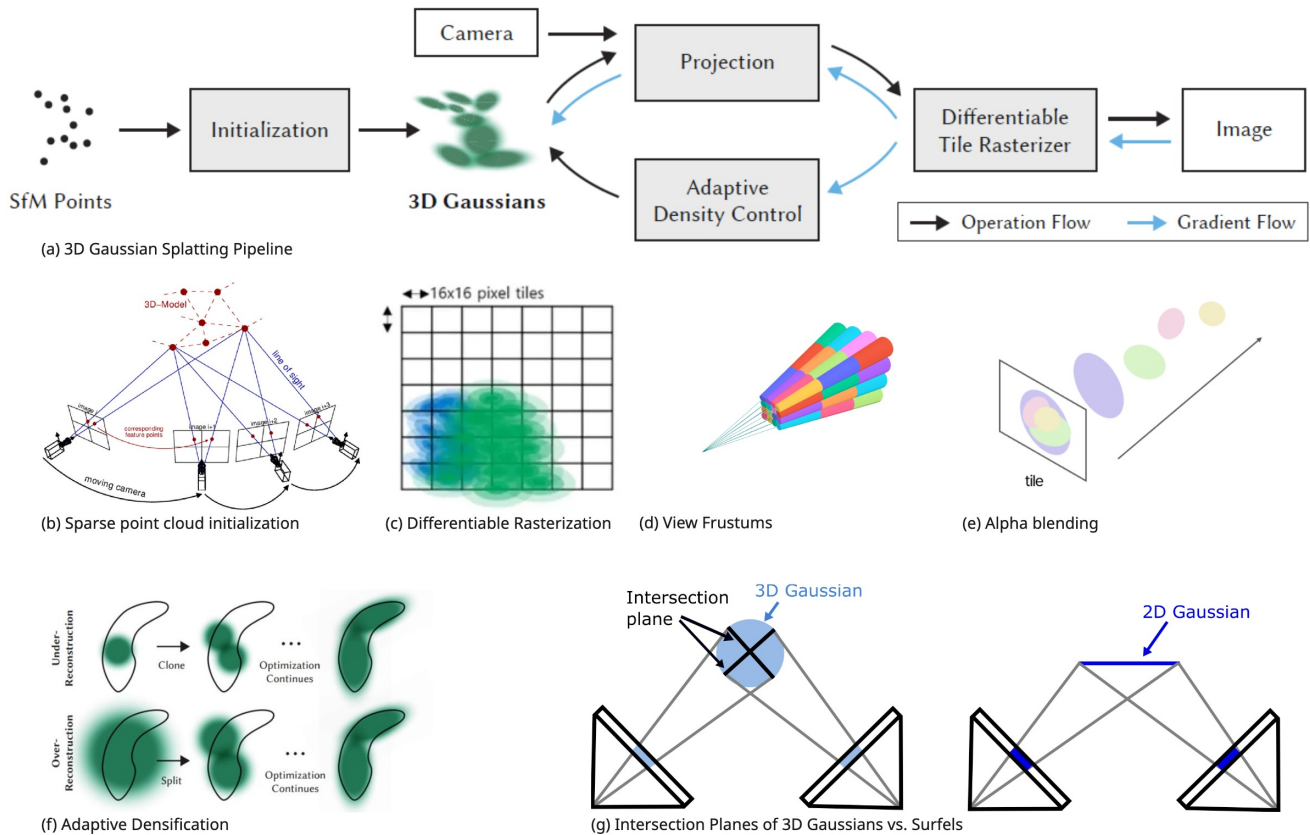


Fig. 2. Visualization of key principles in 3D Gaussian Splatting pipeline (a). Gaussians are initialized from a sparse point cloud (b), for fast rendering the image is split into tiles using differentiable rasterization (c). Projected Gaussians inside a tile’s view frustum are sorted by depth (d), this allows α -blending to determine the final color of each Gaussian (e). During optimization, adaptive densification controls the number of Gaussians to minimize reconstruction errors (f). View-dependency of color can lead to inconsistency when rendering from different views, flattening the z-scale can improve consistency (g). Figure compiled from (a)-[15];(b)-[16]; (c),(e)-[17];(d)-[18];(f)-[15];(g)-[19]

refined through differentiable rasterization-based optimization, point-to-plane ICP alignment [35] or (semantic) bundle adjustments [29, 31, 32, 36]. Coarse-to-fine tracking strategies, optimizing estimates in multiple scales, further boost accuracy and minimize initialization errors [27, 33, 37]. To prevent drift and error accumulation, some systems use keyframe selection with global or hierarchical bundle adjustment framework, ensuring that the estimated camera trajectories remain stable over time [31, 35]. Other methods, incorporate Iterative Closest Point (ICP) techniques and graph-based optimization, leveraging both front-end and back-end processing for large-scale scene reconstruction [33]. While most systems use monocular RGB-D input and adopt optimization techniques, other methods propose the integration of multi-sensor data, such as IMU, LiDAR, or stereo data for improved accuracy and camera pose propagation [31, 38].

Despite these commonalities, differences emerge in the mapping strategies. They vary from coarse-to-fine refinement using sparse pixel initialization and depth-based updates, to silhouette-guided rendering that incrementally refines poses, to dividing the scene into sub-maps for localized optimization [25, 26, 27].

Going beyond static mapping, newer semantic SLAM systems

imbue semantic features directly into Gaussian parameters. This enables joint optimization of semantics, geometry, and appearance in a unified framework [29, 37, 39]. In parallel, dynamic SLAM systems adapt 3DGS to model non-rigid environment such as deformable tissues in endoscopy. These systems integrate temporal deformation fields, occlusion-aware loss function, and surface-aligned regularization to capture motion while maintaining consistent tracking [30, 40, 41]. SLAM in unconstrained environments often deals with sparse observations, occlusion, or ambiguous input. Recent work proposes rendering-guided densification to refine geometry by injecting new Gaussians in underrepresented areas [28]. Other methods reduce the number of splats by modeling scenes with hybrid Gaussians that selectively capture solid vs. transparent structures [33].

c) 3D Gaussian Splatting points: 3D Gaussian Splatting Radiance Field [15], more widely known as 3D Gaussian Splatting (3DGS), is an explicit radiance field-based scene representation that uses 3D Gaussian primitives instead of traditional point clouds. Each 3D point in this representation is not just a simple coordinate, but a learnable 3D Gaussian distribution. More concretely, a Gaussian is characterized by

a covariance Σ and a center (mean) point μ ,

$$G(x) = e^{-\frac{1}{2}(x-\mu)^\top \Sigma^{-1}(x-\mu)} \quad (1)$$

The means of 3D Gaussians are initialized by a set of sparse point clouds (e.g. obtained from SfM). Each Gaussian is parameterized by its center position $\mu \in \mathbb{R}^3$, spherical harmonics (SH) coefficient $c \in \mathbb{R}^k$ (k representing degrees of freedom) for view-dependent color, rotation factor $r \in \mathbb{R}^4$ (in quaternion rotation), scale factor $s \in \mathbb{R}^3$ and opacity $\alpha \in \mathbb{R}$. The covariance matrix Σ describes an ellipsoid configured by a scaling matrix $S = \text{diag}([s_x, s_y, s_z])$ and rotation matrix $R = \text{q2R}([r_w, r_x, r_y, r_z])$ where $\text{q2R}()$ is a function to construct a rotation matrix from a quaternion. The covariance matrix can then be computed as,

$$\Sigma = RSS^\top R^\top \quad (2)$$

To optimize the 3D Gaussian parameters to represent a scene more accurately, they need to be rendered into images in a differentiable manner. Therefore the 3D Gaussian points are projected onto a 2D image plane in a process called splatting [42]. This is done by applying a viewing transformation W and the Jacobian of the affine approximation of the projective transformation J to the covariance matrix Σ to get a projected 2D covariance matrix $\Sigma' = JW\Sigma W^\top J^\top$ in camera coordinates. To achieve fast rendering and allow approximate α -blending, the final image is split into 16×16 tiles (Figure 2 c). Then, for each tile, the projected Gaussian that intersect with the tile’s view frustum are sorted by depth (Figure 2 d). Consequently, at a given pixel the color C is computed by α compositing the opacity α and color c , computed from spherical harmonics parameters, of overlapping 3D Gaussians (Figure 2 e)

$$C = \sum_{i \in \mathcal{N}} c_i \alpha_i \prod_{j=1}^{i-1} (1 - \alpha_j) \quad (3)$$

During optimization, parameters are initialized from SfM point clouds or random values. It employs Stochastic Gradient Descent (SGD) [43] with an L1 and D-SSIM [44] loss function, optimizing against ground truth and rendered views. To address under- and over-reconstruction, periodic adaptive densification is applied, adjusting points with high gradient variations and eliminating those with low opacity (Figure 2 f). This enhances scene representation quality while minimizing rendering errors.

d) Surfels: Surfels, or surface elements, are point-based rendering primitives used to approximate surfaces through oriented point samples enriched with attributes such as position, normal vector, color or texture [45]. Originally presented as an alternative to mesh-based representations with no explicit connectivity and therefore ease of manipulation, this idea resurfaced in recent attempts to address some of the shortcomings of 3D Gaussian Splatting. Despite their efficiency and photorealistic rendering, 3DGS shows limitations with surface reconstructions. 3D Gaussian splats are of volumetric, view-inconsistent nature, therefore limited in accurate geometric representations. To address this, recent methods share a unifying principle of transforming unstructured volumetric splats

into compact, surface-aware, and view-consistent primitives - such as disks, planes, or flattened ellipsoids (Figure 2 g). These methods introduce 2D-oriented Gaussians that lie explicitly on the scene’s surfaces [19, 46] enforced by geometric regularization, e.g. depth-normal consistency or multi-view alignment. A parallel strategy, taking direct inspiration from surfels, collapses the z-scale of 3D Gaussians to create Gaussian surfels, enabling explicit normal encoding and enhanced optimization stability [47]. Beyond geometric fidelity, other approaches emphasize compactness and rendering efficiency. By applying 2D Gaussians ultra-fast image representation and compression can be achieved avoiding volumetric overhead while preserving detail [48]. Other approaches, meanwhile, extend 2D Gaussian Splatting by attaching per-primitive textures, improving on high-frequency appearance modeling and disentangling geometry from texture [49, 50].

C. Impact of input sources

a) Monocular video-based Reconstruction: Reconstructing 3D scenes from 2D videos usually requires multi-view videos to be captured. Although they only see the scene from one view point at a time, depending on the method on how the video is captured, it can still contain cues that are effectively similar to multi-view capture [51].

Traditional 3D reconstruction approaches often perform well under controlled conditions but face challenges in-the-wild, where input data—such as casual monocular videos—exhibit wide variations in lighting, exposure, and camera settings. One strategy to handle such appearance variability is to condition the scene representation on learned appearance embeddings, allowing the color of each 3D point (or Gaussian) to adapt based on the input image. This can be further enhanced by incorporating image-dependent opacity to suppress transient or inconsistent elements across views [52]. Another direction addresses the issue of incomplete or uneven view coverage, common in casually captured videos. Here, generative priors, such as diffusion-based, can guide the synthesis of unseen viewpoints, effectively filling in missing information and improving reconstruction quality [53].

Another problem that arises with in-the-wild captures, is different kinds of blur, such as motion, defocus, and down-sampling blur. These degradations can significantly affect the accuracy of SfM and lead to poor reconstruction results, especially when initial camera pose estimate are unreliable. A common strategy across recent works is to explicitly model the blur to achieve better alignment between rendered and observed frames. One approach simulates the blur by rendering multiple sub-frame viewpoints and averaging them to explain the observed blur [54]. Another incorporates the blur estimation process directly into training by synthesizing blurred from interpolated sharp images, rendered along an estimated camera trajectory [55]. Alternatively, image-space modeling has been proposed, where blur is captured through spatially-varying per-pixel kernels predicted by a dedicated Blur Proposal Network. To improve stability when initializing from sparse point clouds, this approach uses a coarse-to-fine training schedule to refine both kernels and reconstructions

incrementally [56]. Mobile devices often rely on rolling shutter cameras, which capture image rows sequentially. When the camera moves rapidly, it introduces temporal distortions that create warping artifacts, violating the assumption of static global camera poses - a premise in many 3D reconstruction techniques. To address this, a recent work proposes a model that treats camera pose as time-varying during exposure, enabling simulation of these effects [57]. This is achieved by leveraging visual-inertial odometry (VIO) to estimate per-frame velocities, which inform a differential rendering pipeline capable of explaining rolling-shutter and motion blur effects.

b) Handling non-calibrated cameras: In the context of 3D reconstruction, non-calibrated cameras refer to cameras for which the intrinsic and extrinsic parameters are either unknown or not predetermined. These parameters are crucial for accurately mapping 2D images into 3D space and are usually pre-computed from COLMAP [7]. The SfM (Structure-from-Motion) algorithm depends on dense image input, the amount of overlap, and the number of feature correspondence across those images to correctly estimate camera parameters. This process can be, depending on the input, time consuming or fail due to sensitivity to feature extraction errors, difficulties in handling textureless and repetitive regions [58], and sparse input data. To weaken the dependence on SfM algorithms, research presents two main paradigms: pose refinement and pose free reconstruction. Pose refinement methods focus on improving initial, often imprecise pose estimates by optimizing the camera parameters through iterative refinement using 3D scene reconstructions such as 3DGS. These methods work under the condition that initial pose estimates are available, precomputed either through COLMAP or other means. The poses are then refined typically by render-and-compare strategies or 2D-3D feature matching [59, 60]. These methods provide fast and reliable improvements, when initial poses are available but ill poised, however in cases of completely unknown parameters they fail. For this reason, pose free methods try to loosen the dependency on COLMAP, by jointly estimating 3D geometry and camera parameters directly from unposed images. This is achieved through efficient methods like pixel-aligned point maps, depth refinement and matching-aware pose networks [58, 61, 62, 63]. Some methods integrate pretrained vision transformers to initialize point maps and Gaussian primitives and enable scalable training across unordered and large-scale image sets [64, 65]. These strategies enable fully differentiable pipelines that jointly optimize both intrinsic and extrinsic camera parameters along with scene geometry, achieving state-of-the-art rendering and pose accuracy without any precomputed camera input [66].

c) Wide-angle (fisheye) lenses: Most 3DGS frameworks struggled with lens distortion artifacts when processing wide-angle imagery with a large field of view (FOV), leading to noisy and hazy 3DGS reconstructions. A recent self-calibrating framework [67] has introduced a resampling strategy that solves this problem by combining invertible residual networks [68] with explicit grids.

d) Integrating LiDAR and RGB-D data: RGB-D or color-depth cameras are made up of two main components: a standard camera capturing RGB data and a projector-sensor

system capturing depth data. This system can be used in different ways, but the one of interest is to measure distance and shape of any object by projecting structured light on to a scene. This data combined with the color information from the RGB camera can then be used to construct a colored point cloud [69]. Depth data can here improve robustness in ambiguous or textureless scene by providing geometric cues where RGB fails [25, 34]. In many systems depth data is utilized through depth-aware loss terms or direct ICP alignment [27, 31, 35]. Additionally it can be utilized for more precise surface modeling and 3D point placement or constrain 3D structures across different views [28, 29, 33, 39]. A major drawback, however, is the short effective range of depth sensors. LiDAR sensors on the other hand use one or more laser sensors to measure a scene by bouncing laser beam off of objects. The technology is quite mature and often used in the automotive or industrial sectors for distance measures [69]. In a smaller form factor, the technology is also available on certain Apple hand held devices². Without the range limitation of depth cameras, LiDAR can provide precise, and high-range depth data, which can be useful in outdoor or very poorly textured and dark environments [38]. LiDAR points together with RGB data for color can directly be used to initialize 3D point-based representations, like Gaussians, for environments where visual features are sparse or unreliable [38].

e) Domain-free 3D scenes: Recent advances in 3D generative modeling have emerged around 3D Gaussian Splatting (3DGS) as a representation compatible with diffusion-based pipelines. Central to nearly all methods is the integration of 2D diffusion priors, particularly Stable Diffusion variants. Nearly all recent works - spanning from object-level generation [70, 71, 72, 73, 74, 75, 76, 77, 78], scene-level synthesis [36, 79, 80, 81, 82], and 4D content modeling [53, 83, 84, 85, 86, 87, 88] - adopt Score Distillation Sampling (SDS) [89] or closely related guidance techniques to supervise the generation of semantically aligned, view-consistent 3D content from sparse input such as text, RGB, or RGB-D images. A common architectural pattern involves multi-stage generation, where coarse geometry, typically initialized from text [90, 91, 92] or images [72, 93], is refined through optimization [75, 79] or amortized inference [71, 73, 93, 94, 95]. Additionally recent structured representations [90] allow 3D convolution and parameter-efficient training.

A key challenges lies in ensuring multi-view consistency. To enforce spatial coherence across novel views, approaches like patch-level hypergraph reasoning [76], epipolar attention [72], volumetric pruning [73], geometric diffusion [75], and Gaussian alignment losses [87] have emerged, while at the same time, a growing focus on efficiency has led to the reduction of inference time by significant amounts through training free-methods [94], feedforward networks [74, 93], or reduced sampling steps [77, 85].

Beyond object-centric synthesis, several frameworks introduce solutions for scene-level generation with controllability. To this end, many frameworks incorporate layout-aware priors,

²<https://www.apple.com/newsroom/2020/03/apple-unveils-new-ipad-pro-with-lidar-scanner-and-trackpad-support-in-ipados/>

derived from large language models (LLM), to structure object placement, enhance composition, and support interactive editing through semantic inpainting [96] and multi-entity optimization [36, 80, 81, 92]. Panoramic image lifting has further enabled globally coherent 360° 3D scenes [82].

Parallel to static scene generation, 4D generative modeling extends 3DGS, representing dynamic content via deformable Gaussians optimized with spatio-temporal regularization [83, 84, 86, 87]. While some approaches use LLM-guided compositional motion [92], others enforce motion realism from monocular input using neural bone representation [53] or adaptive densification [88]. Notably, to allow modular control and motion transfer, compositional 3D models segment scenes into deformable entities [92], while real-time pipelines [85] focus on acceleration over complexity. Overall, controllability varies from implicit optimization in static generation [70, 73] to explicitly guided scene editing and motion planning [36, 92, 97].

D. Sparse view and reconstruction from a single image

a) Reconstruction from Images: Reconstructing 3D scenes from images can be challenging especially when there is a lack of dense multi-view input (see Figure 3). Constructing high-quality 3D Gaussian Splatting (3DGS) scenes directly from image inputs has become an active research direction, expanding 3DGS from multi-view reconstruction into minimal-view or few image scenarios. Technically these methods can be categorized in to three main approaches: optimization-based reconstruction, amortized feed-forward prediction, and hybrid refinement with generative priors. Optimization-based methods [116, 117] iteratively reconstruct 3D Gaussians with the use of structural prior guidance, such as monocular depth, multi-view flow, or visual hulls. Through these regularized loss terms they can enforce view-consistent geometry and can be optimized through differentiable rendering. In contrast, amortized models [93, 118, 119, 120] focus on training neural networks to directly infer 3D Gaussian parameters from images using convolutional or transformer-based architectures. These models usually incorporate camera pose or ray-based conditioning, and adopt innovative network architectures - for example scan-ordered sequential networks or hybrid token designs - to efficiently scale the prediction to large numbers of Gaussians while preserving fidelity. A third emerging paradigm combines explicit Gaussians with 2D diffusion-based guidance for appearance refinement, occlusion completion, and even editing [121, 122]. These methods begin with a coarse 3D reconstruction and then render multi-view image, which are edited or enhanced using diffusion models. These enhanced views are then used to re-optimize the 3D scene to achieve higher fidelity even with as sparse input as a single image [121, 122, 123]

Although neural 3D reconstruction has made significant progress [125, 126], they usually depend on densely captured multi-view data with well-initialized poses for each frame, e.g. pre-processed with COLMAP [7].

Next generation frameworks, like InstantSpat [127] or Dust to Tower [63] reconstruct 3D scenes from sparse-view images

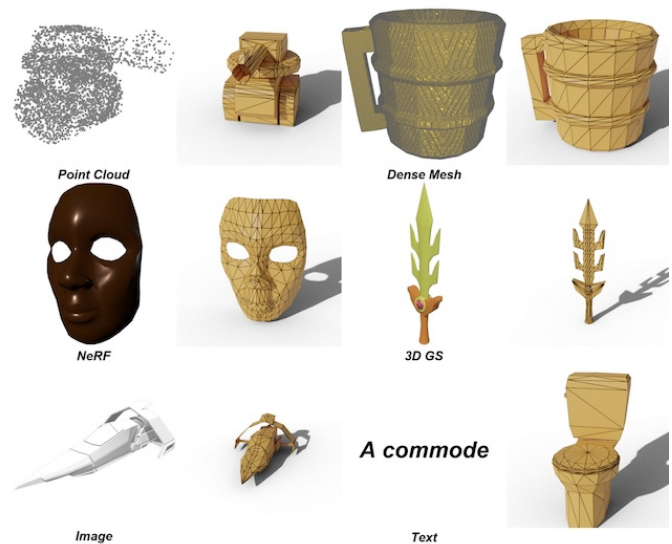


Fig. 3. Generation of mesh models. Image from [124]

without relying on Structure-from-Motion (SfM). However, these methods still use models like DUST3R [128] or MAST3R [129] to predict pixel-aligned dense stereo correspondences between sparse images and initialize camera parameters. They build a co-visibility graph to align stereo point maps across multiple views. Then it jointly optimizes 3D Gaussian Splatting representation and camera poses using gradient-based photometric error minimization. Additionally they use Monodepth models, like Depth Anything V2 [130] for depth estimation from a single image.

Ultimately, fully interactive Digital Cousin [1] scenes can be generated from a single RGB image. Digital Cousins [1] are scenes that, unlike Digital Twins, do not exactly replicate real-world counterparts but retain key geometric and semantic affordances. Open vocabulary objects [131, 132] in the RGB image are identified using GPT-4. GroundedSAM-v2 makes a segmentation of the identified objects. Depth information is estimated using Depth Anything V2 [130]. Extracted 3D objects are matched to digital assets from a dataset (e.g., BEHAVIOR-1K [133]) with CLIP similarity scores and DINOv2 embeddings to find the best-matching digital assets. The closest matches are selected, assigned appropriate orientations, and placed in a physically plausible scene. Objects are adjusted to remove physical penetrations and ensure stability. CAST [108] offers several improvements over the concept of Digital Cousins [1]. CAST’s primary goal is to recover high-quality 3D scenes with detailed geometry, vivid textures, and physically sound interdependencies with physics-aware correction step. CAST [108] is a generation-driven scene reconstruction approach where 3D meshes for individual objects are generated and then aligned, while Digital Cousins rely on retrieving existing 3D assets from a dataset. SINGAPO [134] has a similar pipeline as Digital Cousins [1], however, SINGAPO [134] is focused on generation of articulated parts of household object from a single image, like refrigerators, cabinets, or microwaves.

Another line of works tackle both tasks of 3D object

TABLE II
SUMMARY OF OBJECT-LEVEL SINGLE-VIEW 3D SCENE RECONSTRUCTION AND MODELING METHODS.

Method	Framework	model arch.	Inter. 3D rep.	Strategy	OV	SO	Appera.	RL
3D scene reconstruction								
Total3D [98]	end-to-end	2D CNNs	template mesh	supervised	✗	✗	✗	bbox
IM3D [99]	end-to-end	2D CNNs, GCN	SDF	supervised	✗	✓	✗	bbox
[100]	end-to-end	2D CNNs	voxels	weakly supervised	✗	✗	✗	✗
InstPIFu [101]	end-to-end	2D CNNs	implicit function	supervised	✗	✓	✗	mesh
Uni-3D [102]	end-to-end	TFs	SDF	supervised	✗	✗	✗	mesh
SSR [103]	end-to-end	2D CNNs	SDF	supervised	✗	✗	✓	✗
Gen3DSR [104]	modular	FMs	neural field	zero-shot	✓	✗	✓	mesh
MIDI [105]	end-to-end	TFs	latent feat.	diffusion	✓	✗	✗	✗
Deep Prior Assembly [106]	modular	FMs	mesh	zero-shot	✓	✗	✓	✗
[107]	modular	UNet, TFs	3DGS	diffusion	✗	✗	✗	✗
CAST [108]	modular	FMs	latent feat.	diffusion	✓	✓	✓	✗
3D scene modeling								
IM2CAD [109]	modular	2D CNNs	-	supervised	✗	✓	✓	bbox
Mask2CAD [110]	end-to-end	2D CNNs	-	supervised	✗	✗	✗	✗
Patch2CAD [111]	end-to-end	2D CNNs	-	supervised	✗	✗	✗	✗
ROCA [112]	end-to-end	2D&3D CNNs	NOCs	supervised	✗	✗	✗	✗
PSDR-Room [113]	modular	FMs	PC	zero-shot	✓	✗	✓	planes
DiffCAD [114]	modular	FMs	PC & NOCs	diffusion	✗	✗	✗	✗
Digital Cousin [1]	modular	FMs	PC	zero-shot	✓	✓	✗	planes
Diorama [115]	modular	FMs	PC	zero-shot	✓	✓	✗	planes

retrieval and object alignment to the image in a pipeline of creating synthetic 3D scene [109, 110, 111, 112, 135], where objects are detected, segmented [136], aligned, and CAD models are retrieved and posed to form a 3D scene. These works typically require large-scale data of image-CAD pair annotations to train the model in an end-to-end manner, which makes them hard to generalize due to tremendous efforts needed to collect expensive data. Recently, several zero-shot methods [1, 115] have been proposed to mitigate the problem of scene data scarcity by leveraging visual foundation models and Large Language Models (LLM). Digital Cousin [1] simply ranks 3D object candidates using DinoV2 [137] features on multi-view renderings and ask GPT4o to pick the top-K best matching ones. Diorama [115] proposes a hierarchical retrieval strategy where both text and visual modalities are employed for better retrieval results using DuoDuoCLIP [138].

E. Retrieving Object Mesh Models

Typical 3D shape retrieval measurements require both the ground-truth shape and retrieved 3D shapes to compute either retrieval accuracy or point-based reconstruction scores, such as Chamfer Distance (CD), Normal Consistency (NC) and F-score $F1^t$ conditioned on point-wise distance t that indicates the strictness of points being accurately reconstructed. These metrics can be directly used as shape similarity to retrieve 3D shapes given an object point cloud as query. We note that point-based metrics are sensitive to the point sampling method and the number of sampled points. The work [139] shows that Under the same sampling condition, NC and $F1^t$ tend to

rank unrelated shapes higher compared to CD, which either present distinguishable geometric structure or have wrong categories. Overall, CD is a more robust point cloud-based similarity score for shape retrieval that outputs reasonable shape ranking without the need to tweak hyperparameters. Besides 3D representation with explicit geometry such as point clouds and voxel, 3D shapes can also be represented as multi-view images. A prescribed approach [140] represent a 3D shape as light-field descriptor (LFD), computed from a set of pre-rendered binary masks, and retrieve the target shape by comparing L1 distance of features.

More recently, learning-based methods are developed to advance the progress in different variants of the 3D shape retrieval task, involving querying of shapes from single-view images [110, 111, 141, 142], text [143, 144], voxels [112], point clouds [145] and other 3D objects [146]. To align the different modalities of the same physical entity, queries and 3D objects are usually encoded into a joint-embedding space that learnt in an end-to-end manner using triplet or contrastive losses. In such case, retrieval can be achieved by fetching the 3D object with the minimal distance in the high-dimensional embedding space to the query object. The distance is usually measured by L2 norm or cosine distance. Given an image query of the target object, CMIC [141] achieves state-of-the-art performance on retrieval accuracy by using instance-level and category-level contrastive losses. To handle different texture and lighting conditions in images, [147] proposed to synthesize textures on 3D shapes to generate hard negatives for additional training. [148] used a deformation-aware embedding space

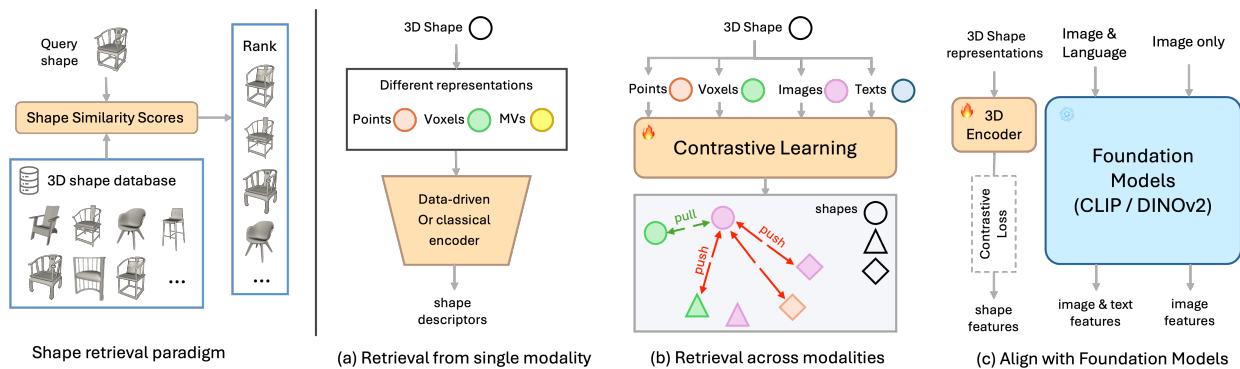


Fig. 4. Summary on 3D shape retrieval paradigm.

so that retrieved models better match the target after an appropriate deformation.

The natural limitation of learning a image-CAD joint-embedding space is that it would consume large-scale image-shape pair annotations to achieve generalizability to novel object instances and categories, which is empirically infeasible and expensive. One promising solution is to investigate the use of vision-language model (CLIP [149]) to guide the alignment of 3D shape embeddings. ULIP [150] is one of the pioneers that align text, image and 3D modalities. It uses frozen CLIP text-image encoders, and trained only the point-cloud encoder. However, the generalizability of these works were limited by the available dataset size at the time. OpenShape [151] and ULIP-2 [152] are among the first to scale up paired text-image-3D training data to train a point cloud encoder aligned with the CLIP embedding space multi-modality contrastive learning. They take advantage of combined large-scale 3D shape datasets [153, 154] to recover real-world data distribution beyond a fixed number of classes and pretrained LVLMs (GPT-4v) for rendering captioning to generate paired text description. Uni3D [155] maps point cloud patches to image patches within pre-trained ViTs to align the 3D point cloud features with the image-text aligned features. In contrast to aforementioned existing works, DuoDuoCLIP [138] learns shape embeddings from multi-view images instead of point clouds that show better generalization performance and more light-weight hardware requirements.

III. LIGHT AND REFLECTIONS

A. Relighting

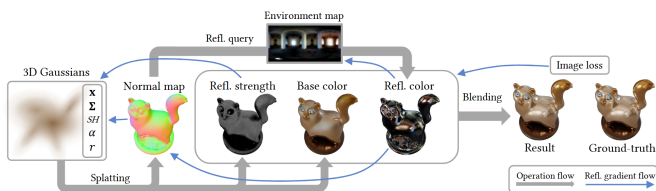


Fig. 5. Example rendering pipeline for Gaussian splatting with reflections [156]

One of the crucial aspects of the digital twin environments is the ability to impact the scene lighting (to simulate different

conditions like time of day). While the spherical harmonics used in the Gaussian Splatting allow for some view-dependent color modeling, information about the whole scene lighting is baked into them and the basic rendering pipeline doesn't allow for any light modifications. This problem was identified quickly after the 3DGS publication, with authors expanding the rendering pipeline to mimic the Bidirectional Scattering Distribution Function³ (BSDF) process [157, 158, 159]. This physical-based approach expands Gaussians with a set of additional, learnable appearance parameters (albedo color, roughness, normal vector direction), with the environment lighting modeled as an additional, global texture. This texture, when changed during the rendering, opens the possibility to directly impact the scene lighting (the exemplary pipeline of such a system is presented on Fig. 5). Further works focused on better modeling of indirect lighting. In [160], based on the simple single-bounce ray-tracing the color is sampled either from the global texture or from the set of spherical harmonics trained to model per-Gaussian indirect lighting. Even better effects are achieved after switching to deferred rendering process⁴ [156, 161, 162], allowing for an accurate, per-pixel shading with additional reflection effects, and even adding the explicit point- and directional-light sources [163]. A similar approach with the BSDF pipeline and deferred rendering can be also used with 2DGS [164], providing additional surface-based regularization [165], with extra local mesh reconstruction to achieve better surface quality and reflections [166] To further enhance the quality of surface-lighting disambiguation, some authors utilize multiple different lighting conditions during the training phase. First approaches used single point-light per image [163], and newer solutions require as little as two different global-lighting sets [167]. While the explicit, BSDF-based surface appearance modeling is most popular, there are also attempts to model the view-light-surface dependence using the implicit, trainable latent feature per Gaussian [168]. During the rendering phase, this latent feature is decoded using the light- and view-directions as conditioning inputs.

³A BSDF, or Bidirectional Scattering Distribution Function, is a mathematical model that describes how light scatters when it hits a surface, relating incoming and outgoing light directions and intensities. It's a fundamental concept in physically based rendering (PBR) and is used to simulate realistic material appearances

⁴https://en.wikipedia.org/wiki/Deferred_shading

TABLE III
COMPARISON OF MAIN FEATURES OF DIFFERENT RELIGHTING APPROACHES (VALUES FOR SHADOWS COLUMN: RT - RAY-TRACED, AO - BAKED AMBIENT OCCLUSION)

Method	Dynamic lights	Shadows	Rendering	Representation
Relightable 3DGS [157]	no	RT	forward	explicit
GS-IR [158]	yes	RT+AO	forward	explicit
GaussianShader [159]	no	no	forward	explicit
GIR [160]	no	RT	forward	explicit
DeferredGS [161]	no	no	deferred	explicit
3DGS-DR [156]	no	no	deferred	explicit
GI-GS [162]	no	RT+AO	deferred	explicit
GS ³ [163]	yes	RT	deferred	explicit
GS-ID [165]	yes	AO	deferred	explicit
Reflective GS [166]	no	RT	deferred	explicit
ReCap [167]	no	no	forward	explicit
RNG [168]	yes	RT	deferred	implicit

Table III presents a comparison of the important aspects of all aforementioned methods.

In the context of a digital twin environment generation, all of the methods lack one, important characteristic. They rely on a single environment map, global for the whole scene. In many indoor scenarios, where we have multiple rooms, each of them is usually different in terms of lighting. This could be addressed by learning per-room environment map and selecting the proper environment during the rendering phase.

B. Mirrors

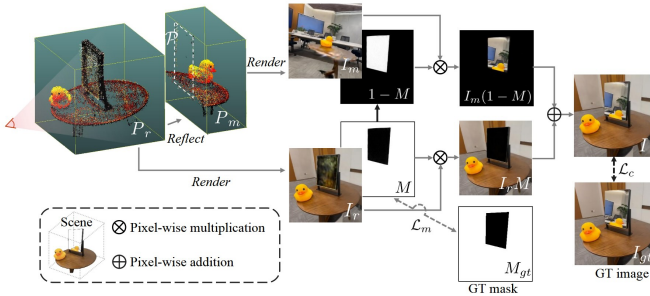


Fig. 6. Overview of MirrorGaussian [169].

While the approaches presented above are good enough to model the shiny (specular) surfaces, mirrors still pose a challenge for them. Learned environment lighting map is usually of low resolution and can't capture sharp object reflections. In the traditional 3D Gaussian Splatting, the mirror is ignored in the sense that the reflected scene is modeled as another room (if the mirror is on the wall and there are no views from the other side). If the mirror is placed in the middle of a scene, the reflections are usually encoded in the color SH and tend to be very blurry. One of the common approaches to solve this problem is to detect parts of the scene that are actual mirrors and render the scene from virtual camera placed "on the other side" of the mirror [169, 170, 171] (Fig. 6 present a sample rendering pipeline with a single mirror). Those approaches rely on availability of mirror masks in the training dataset (either hand-drawn or detected automatically [172]). The mirror plane

is calculated either on the initial stage from the SfM point-cloud [169] or from the Gaussians created in the first stage of the training from the set of masked input images [170]. The second training step (using full, unmasked images, after fixing the positions of Gaussians) is devoted to the reflection refinement, either by modification of mirror plane [170] or virtual camera position [171]. The natural extension to the presented approaches is to allow semi-transparent reflections (i.e. glass). GlassGaussian [173] expands the Mirror3DGS to work with semi-transparent glass surfaces. The angle-dependent reflection strength is modeled with an additional spherical harmonics parameter, and the scene is rendered in multiple passes: transparency first, and the mixed with the reflection rendered with the virtual camera. Those approaches allow for the dynamic scenes, as the reflected part of the scene is actually rendered, and not encoded in the Gaussian color parameters (in contrast to [174, 175], which produce good results but only for the static scenes).

IV. TEMPORAL DYNAMICS

A. Temporal dynamics of 3DGS

1) *Dynamic scene representation*: Different approaches are being adopted in order to represent a dynamic scene in volumetric rendering approaches. Summary of evolution of the representation is given in Fig. 7.

a) *Implicit neural representation*: One basic approach use and implicit representation of neural network (mainly MLP) to represent both spatial and temporal axes. In [176] a single network was used to encode both spatial and temporal structure, however sophisticated learnable time encoding using time-invariant latent codes. In [180] the temporal information is embedded into a separate deformation network computing coordinate transformations in time to find mappings in the static canonical configuration represented by different network.

b) *Voxel-grid representation*: Implicit approaches are often replaced by more explicit representations using supported voxel-grids. Creating spatio-temporal voxel grids is infeasible due to memory consumption, so usually some hybrid approaches are proposed. In [181] a small deformation network is used to compute point transformations, appropriate

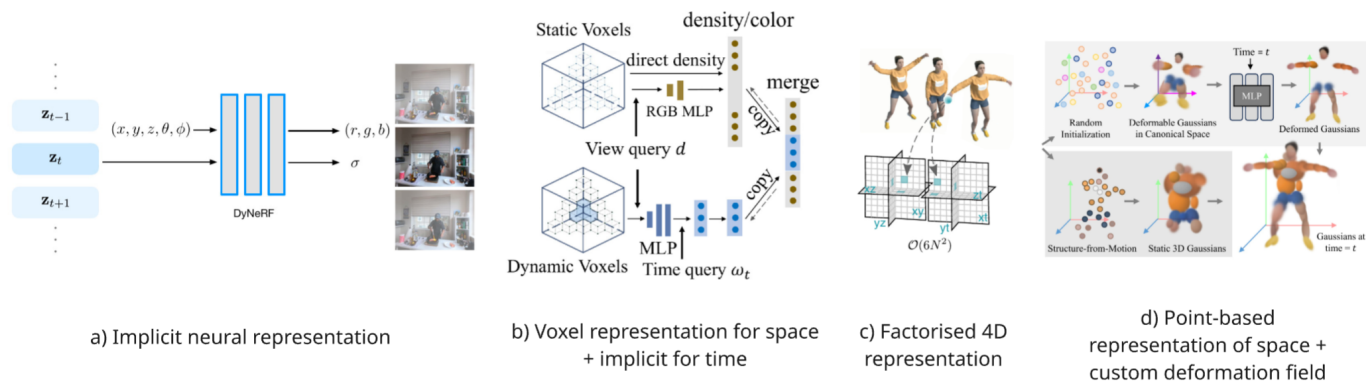


Fig. 7. Evolution of representation methods for dynamic content utilizing differentiable volumetric rendering. The concepts involve fully-implicit representation by neural networks (a), voxel-based 3D representation supported by implicit dynamics (b), fully 4D voxel-based representation using factorization for tractability (c), point-based representation of space (typically by Gaussians) with different methods for representation point dynamics (d). Figure compiled from [176, 177, 178, 179]

positions are sampled from the 3D voxel-grid (representing canonical configuration), but time component is further used in the final radiance network (so the temporal information is in both deformation and radiance networks. Similar approach, but with no explicit deformation field is proposed in [182]. Points at x, y, z coordinates are directly queried in voxel-grids for texture and density to obtain associated features and time component is appended afterwards, before applying radiance field networks. This structure means that some temporal information must be embedded directly into features from texture and density volumes (in addition to radiance networks).

c) Planar factorizations of voxel grids.: Spatio-temporal voxel grids can be approximated from simple structures like planes. In order to maintain compact memory fingerprint the approaches [178, 183] maintain spatio-temporal information in the form of planes (XY, XT, YZ etc.) which can be regarded as 'projections' of the full spatio-temporal voxel grid. The methods differ in representation details. In [178] each matrix element contain a full feature vector independent of its neighbors, while in [183] plane elements are coefficients for a fixed set of basis vector (in the latter cases a number of different basis vectors and different matrices for each plane must be maintained). Grid decomposition into planes can also be used in conjunction with different rendering techniques such as Depth Peeling. In [184] a circular blob is assigned to a voxel grid with learnable radius and density. Learnable features are efficiently obtained via K-planes model. A depth-peeling rendering technique (similar to splatting) is used. Another application of this type of is the modeling of deformation. In [185] the initial set of Gaussians building a scene is modified using data stored in a K-planes model further processed by MLP networks. The Gaussian splatting rendering technique is used.

d) Point-based representations.: Point-based approaches form another category of methods. The scene is typically represented by an unorganized set of Gaussians and different techniques are used to model their temporal dynamics. The Gaussian Splatting technique is used for effective rendering. There are number of approaches that share this characteristic

like [87, 91, 179, 184, 186, 187, 188, 189, 190].

The dynamic models are typically encoded as a deformation field and various approaches are used in this regard. The deformation field can be represented by MLP network [91] sometimes in conjunction with K-planes factorization [185]. In [186] the animation is obtained by modeling variable Gaussian density over time supported by polynomial motion model. Trajectories of individual Gaussians can be encoded on a point-by-point basis [187]. Trajectories can be encoded more efficiently if they are expressed by a limited number of MLP-learnable base trajectories [189] or the dynamic of a dense cloud of Gaussians is represented by a weighed dynamic of a limited set of control points [190], [87] (also MLP driven). A completely different approach was proposed in [188], where in order to represent temporal dynamics, the scene is represented by a set of fully 4D spatio-temporal Gaussians.

e) Decoupling of static and temporal information.: An observed common way to handle a complexity of creating spatio-temporal model is decoupling of storage for static spatial structure (called canonical configuration) and object dynamics. It is often done by specifying a separate deformation function in addition to the structure storing initial spatial information for a static scene. This kind of approach is used in most solutions with some notable exceptions, such as mentioned [176] where only a single network is used for both spatial and temporal information or [188] where the spatio-temporal scene is modeled by fully 4D spatio-temporal Gaussians. Such spatio-temporal Gaussian volume can be projected into an xyz time-slice in order to perform Gaussian Splatting optimization.

B. Regularization of motion patterns

In natural video sequences there exist strong spatio-temporal correlations of the data. More often than not a continuity and smoothness of motion is maintained over a sequence. Situations when an object "appear out of nowhere" are quite rare. Also the locality of motion is quite common characteristic. The near-by points constituting objects tend to

follow similar motion patterns and in short-time windows can be even regarded as rigid objects.

Taking into account typically observed motion constraints can be beneficiary. Having more constraints may result in smaller number of parameters for motion representation and also enable effective learning from much less data. While data-driven approaches using smaller number of spatio-temporal constraints can be effective in multi-camera setups, more model-oriented approaches with stronger constraints are usually better suited for monocular data acquisition.

a) Regularization by representation.: Dynamic scene representation can be a useful tool for ensuring smoothness in spatial and temporal domains. Vanilla 4D voxel-based representation assumes independence of particular voxels. However, 4D voxel-spaces represented as a factorization of simpler structures like planes contain inherent assumption regarding correlations of voxels in out-of-plane directions which represent either spatial or temporal correlations in the data. This property was exploited in approaches based on K-Planes [178, 185] and Hex-Planes [183] representations. This type of explicit modeling of correlations is typically further supported by appropriate loss functions. Different type of representation-based regularization was proposed in [188]. Full 4D Gaussian (spatio-temporal) representation adopted in this solution supports motion smoothness and coherence, providing that Gaussians are enough coarse-grained.

Point-based representations can also be designed in a way to impose some constraints on the motion and introduce certain order to motion estimation. Good examples are approaches that base on projecting individual motion patterns on a small number of learnable template motion trajectories (called motion representation fields) [189]. Due to per-point sharing of base trajectories, the method is provide constraints to the motion field leading to faster and more reliable optimization. Similar goal is achieved in related approaches [87, 190] where templates are formed by a small subset of control points, for which trajectories are established by a trainable neural network, while the positions and rotations of Gaussians in time are governed by near-by control points using Linear Blend Skinning principle.

b) Regularization loss functions.: Another, and more general way to impose constraints and smoothness on motion is by applying custom loss functions during training. One approach is the regularization imposed on the features stored in grid-like representation. In [178] the K-Planes representation of spatio-temporal volume is accompanied by appropriate regularization losses. While Total Variation in Space component of the loss is responsible for ensuring smoothness in spatial dimensions, a special Smoothness in Time component is established specifically for the temporal dimensions. This component is in the form of 1-D Laplacian in order to prevent fast accelerations in time domain.

The approaches based on Gaussian representation as intrinsically less constrained are often subject to regularization loss functions. In order to obtain good tracking properties of the system the authors of [187] introduce 3 auxiliary loss functions in addition to the standard image reconstruction error: the local rigidity of motion in short time window, similarity of near-by

Gaussians' rotations in short time window and the long-term isometry loss preventing near-by Gaussians to drift apart over longer time intervals.

While representation of motion by a superposition of limited number of trajectories [189] or the motion of limited number of control points [190], [87], imposes certain constraints on motion patters, it can be further extended by appropriate loss functions. E.g. in [189] two additional loss functions are introduced to ensure that arbitrary point trajectory is not dependent on too many template trajectories. Also, the rigidity of motion is supported by the loss enforcing near-by points to have similar trajectory coefficients. In [190] ARAP (As Rigid As Possible) principle is used to achieve similar goals. First a rotation matrix is estimated that best superimpose two temporal configurations of near-by points, then the (ARAP) loss function computes distance errors for this superimposition.

C. Efficiency considerations of temporal methods

The temporal modeling methods based on NeRF, due to increased size of input data, suffer from even greater performance hit then their static counterparts. The time required to train for the network in [180], [176] is measured in days and single frame inference in dozens of seconds. A part of this computational inefficiency originates from the complexity of implicit representation of density and color by a neural network. More recent approaches use voxel grid to explicitly encode at least spatial structure of the scene [177, 181, 182]. This representation enables performance of fast spatial queries and significantly reduce training time below 1h on DNeRF dataset [180] (except for [182] where the training takes several hours) and inference time to order of magnitude about 1s (or even less [177] when filtering static parts of the scene).

The concept of voxelization of the representation is further enhanced into a fully spatio-temporal modules, [178, 183, 184]. For memory tractability such volumes are usually represented using factorization into simpler structures (e.g. 2D matrices). Such solutions [183],[178] give comparable or better training times (dozens of minutes on simpler datasets [180] or several hours on more complex datasets [176]). When paired with efficient rendering technique (hardware-supported differentiable depth-peeling) even real-time rendering performance can be achieved [184].

Gaussian splatting rendering technique provides a boost to the rendering as well as training speeds. This category of methods is able to achieve times below 1h even on complex datasets and a real-time rendering speed [91, 185, 186, 189] with several methods easily surpassing 100 fps.

D. Applicability of temporal methods in robotics

There are several qualities that can be found important for applicability of scene reconstruction method in robotics. 1) the method efficiency, so the methods can work real-time at the inference stage and at least near-real-time at learning stage, 2) ability to work on a sparse set of cameras (ideally in monocular setup), 3) ability to track scene points.

TABLE IV
DATASETS RELATED TO ARTICULATED OBJECTS OR SCENES WITH STATISTICS.

	Source	Clean mesh	Scene-level	Image	Appearance	# categories	# objects	# articulated parts
RPM-Net [191]	synthetic	✓	✗	✗	✗	43	969	1,420
Shape2Motion [192]	synthetic	✓	✗	✗	✗	45	2,440	6,762
PartNet-Mobility [193]	synthetic	✓	✗	✗	✓	46	2,346	14,068
AKB-48 [194]	real	✓	✗	✗	✓	48	2,037	-
OPDReal [195]	real	✗	✗	✓	✓	8	284	875
MultiScan [196]	real	✗	✓	✓	✓	20	10,957	5,129
GAPartNet [197]	synthetic, real	✓	✗	✗	✓	27	8,489	1,166
ACD [198]	synthetic	✓	✗	✗	✓	21	354	1,350

Regarding the first point, the most recent methods based on Gaussian Splatting such as [91, 185, 186, 189] seem to currently offer the highest speed in rendering (over 100 fps) but also in training. These methods are iterative, so they can be safely stopped before a full convergence to quickly obtain a map with lower level of details.

The ability to work on a sparse set of cameras is not always explicitly discussed in the papers regarding the topic. The structure of both NeRF and GS-based methods are based on multi-view optimization does not inherently define the number of required camera inputs, however some methods may be more suitable than the others for monocular environment. One of the commonly evaluated monocular dataset is DNeRF [180]. Most of the prominent GS methods were evaluated on this dataset [91, 179, 185, 188, 189, 190].

The methods evaluated in multi-camera setups are e.g. [184, 186, 187]. Since single camera setups induce less input data, the methods handling monocular inputs often put pressure on applying motion regularization techniques like control points [179, 190], shared motion trajectories [189], 4D Gaussians [188] or deformation field factorization [185].

Point 3) - the ability to track scene points is important from the perspective of estimating object motion and articulation in a dynamic scene. While most GS splatting methods due to particle-like structure of the scene this ability is expressed naturally, there are some approaches like [179, 187, 189, 190] the incorporate the objective of tracking more explicitly and incorporate strong regularization on Gaussian particle motion. While most GS solutions assume the motion field affecting Gaussian position, size and orientation, there is a notable exception [186] where also opacity is subject to a temporal change (which gives an effect of appearing and disappearing Gaussians over time). While the latter approach is good for animation and rendering it might not be effective for tracking.

E. Articulated parts of objects

Articulated objects, composed of multiple rigid parts connected by joints, encompassing a wide range of objects, such as human bodies, mechanical assemblies, furniture, etc. The reconstruction or generation of articulated objects aims to comprehend and represent the shape and mobility of articulated components.

Articulated object reconstruction. The goal of articulated object reconstruction is to recover the 3D geometry and motion

parameters of the objects from various observations. The challenges involve decomposing the part into articulated components and producing the reconstructed surface that can be animated into different articulation states. The input modalities include point clouds, multi-view RGB or RGB-D images, and RGB videos. A line of work focuses on reconstructing the whole object as a single deformable surface either over time or given different states [199, 201, 202, 203, 204, 205]. Another line of work reconstructs each part as separate surfaces interconnected by joints to enable articulation [206, 207, 208, 209, 210].

A-SDF [202] was the first to reconstruct articulated objects using signed distance fields from a single snapshot, allowing deformation into different articulation states. [203] share the same goal with A-SDF but take multi-view RGB images as input for the reconstruction, while CARTO [199] further extends the input to a single stereo RGB image. These works assume the object has only one movable part. LEIA [205] reconstructs the interpolated state of the object between the two given input states from multi-view images without knowing the number of moving parts. These works reconstruct the articulated object as a single unified surface or as an implicit deformation field. The lack of part-level structure in the output geometry makes it difficult to be simulated in a physical simulation software.

To address the part-level reconstruction, CLA-NeRF [206] proposes to reconstruct the object from a few multi-view RGB images of an unseen 3D object instance within the known category. It assumes that the object category is known and all the instances in the category share the same articulated structure. To avoid the reliance on object category, Ditto [207] reconstructs from a pair of point clouds, while PARIS [208] take multi-view RGB images observing the object in two states as input. [209] extends the setting of PARIS to multi-view RGB-D images and reconstruct multiple articulated parts in the output. These works assume the number of articulated parts is known at inference time. In a more flexible setting, Real2Code [210] proposes to reconstruct articulated parts from multiple unposed RGB images of the object in an opening state, and focuses on certain categories of objects that mostly have cuboid-like parts but with no assumption on the number of articulated parts.

Articulated object generation. This line of work aims to synthesize the articulated objects in both geometric and kinematic structures from random noise or user-specified con-

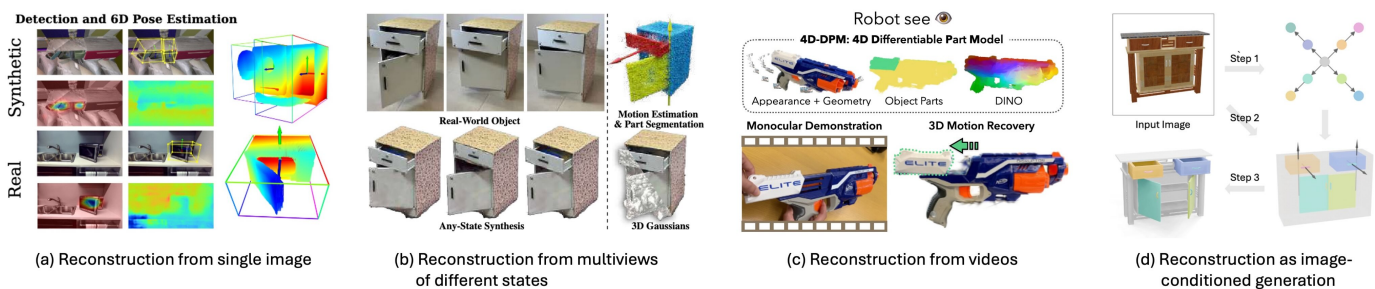


Fig. 8. Summary on articulated object reconstruction from different visual input. Figure reproduced from original paper [134, 199, 200, 201].

straints. NAP [211] is a pioneering work that generates a full description of the articulated object, including part geometry, articulation graph, and joint parameters from random noises unconditionally. CAGE [212] extends the task in a conditional setting, where the object category and a part connectivity graph as given as the user-driven input. The output of these works targets the mesh representation composited in varied structures. SINGAPO [134] and ArtFormer [213] further introduce different controllable generation setting where SINGAPO enables single-image-conditioned generation, and ArtFormer focuses on text-driven generation. ARTICULATE-ANYTHING [214] proposes a general framework that automates the articulation of objects from different input modalities, including text, images, and videos. Programs are used to arrange the part geometries and predict articulation with a specialized mechanism designed to ensure the plausibility of the generated object.

SINGAPO [134] is focused on generation of articulated parts of household object from a single image, like refrigerators, cabinets, or microwaves. The pipeline consists of three progressive steps: Inferring the part connectivity graph from the image using GPT-4o models with in-context learning to predict the connectivity graph of articulated parts from the input image; Structuring the parts using a graph with masked attention of transformer-based diffusion model; Collecting meshes from a part shape library to assemble the final object based on the outputs from previous steps.

V. EXTRACTING PHYSICAL PROPERTIES FOR AVAILABLE SIMULATORS

Extracting physical properties from videos to utilize in physics simulations is a critical step in creating an accurate digital twin. This chapter examines the essential elements needed to accurately simulate a scene within a physics-based environment [5]. We start by summarizing the most popular and recent simulation software across various domains, ranging from simple physical scenes with just rigid bodies and contact interactions to more complex situations involving multi-joint bodies, from soft bodies to fluid dynamics. The chapter investigates how characteristics such as mass, inertia, friction, and viscosity can be derived from video data into a scene description or 3D Gaussians.

A. Physics Simulation for Digital Twin

Recently, physics simulations have seen significant improvements, becoming faster, more reliable, and more comprehensive. They now span a wide array of applications in robotics, industry, and healthcare. This subsection examines the most advanced and widely-used simulation technologies, along with their scene description format. This will highlight the expected outcomes of the video data necessary to accurately create a digital twin.

1) *State-of-the-art Simulation Technologies:* According to [215], the leading physics engines for robotics applications as of September 6, 2023, ranked by frequency of publication, are MuJoCo [216], Gazebo [217], PyBullet [218], Webots [219], and Brax [220]. These engines are optimized for performance, focusing primarily on the dynamics of rigid bodies and multi-joint systems, and support both URDF and MJCF formats. They are widely used in physics-based reinforcement learning research.

For soft body simulations, especially in medical contexts, SOFA [221] stands out. It offers high modularity through customizable modules and libraries, facilitating complex interactions such as cutting [222] and manipulating soft arms [223]. SOFA employs Finite Element Methods (FEM) and requires a meshed discretization of simulated objects. It uses a scene graph structured as a Direct Acyclic Graph for scene importation, detailing mechanical properties and numerical tools, but does not support URDF or MJCF conversions.

ProjectChrono [224] excels in particle simulations and granular dynamics, particularly supporting vehicle simulations for both wheeled and tracked vehicles. It uses the Discrete Element Method (DEM) to simulate large granular systems efficiently on GPUs. ProjectChrono organizes its scenes in JSON format and includes an URDF parser, with the US Army employing it for vehicle simulations.

In the realm of photo-realistic graphics engines, Isaac Sim [225], Unreal Engine, Unity [226], Godot, and Blender [227] are recognized for their high-fidelity visual rendering. Isaac Sim, developed by NVIDIA, utilizes PhysX for physics simulation and is tailored for robotics reinforcement learning. Unreal Engine and Unity, primarily game engines, also find applications in robotics, with implementations like CARLA [228], URoboSim [229], and RoboKudo [230]. Unity further enhances its capabilities by supporting MuJoCo as a physics plugin. Most of them support importing scene from USD format.

Depending on the specific application domains, multiple

physics simulations can be utilized. Recently, Genesis [231] has integrated multiple physics solvers and their interactions into a cohesive system. It features a modular design that includes several generative modules, each dedicated to processing different data modalities, all orchestrated by a high-level agent.

Each simulation platform offers unique advantages and limitations that directly impact the effectiveness of algorithms tailored for specific applications. Algorithms focused on perception benefit from simulators with photo-realistic rendering capabilities, whereas those involved in physics control require simulators that provide detailed APIs for dynamics control, like applying joint torques or forces. For more complex simulation tasks, such as cutting or pouring, the use of FEM or DEM is crucial.

2) *Scene Description Formats*: A robotic scene description is a file format used to describe the configuration of a scene for simulation purposes. Typically, each simulation software employs its own specific scene description format [232], such as MJCF for MuJoCo, SDF for Gazebo, and PROTO for Webots... (see Figure 9). This variety can lead to compatibility issues when a scene described in one format needs to be simulated in a different software environment. As a result, URDF has become widely adopted as a standard format for importing rigid and multi-joint bodies [233]. However, URDF is limited to modeling rigid bodies with only basic constraints and lacks support for complex dynamics such as damping and friction. As a result, it is not suitable for representing soft bodies or fluids. Additionally, URDF does not include photorealistic rendering features for camera simulations; it is primarily intended to define a robot’s visual appearance and collision models using standard joint types.

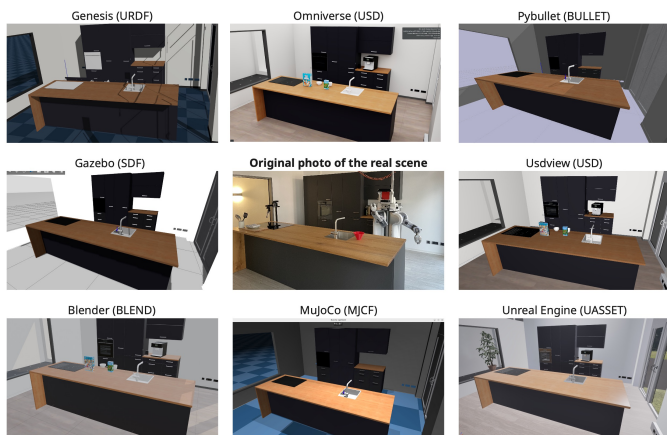


Fig. 9. Different simulators and their scene descriptions, generated from a real environment

To address the limitations of URDF in depicting more complex scenes that include photorealistic rendering properties, the Universal Scene Description (USD) [234] has recently been introduced as a standard format for scene descriptions. Developed by Pixar, USD forms the backbone of Pixar’s 3D graphics pipeline and is utilized in every 3D authoring and rendering application. Originally used in animation studios, USD can describe various domains, including rigid bodies, soft bodies,

and fluids. It is the only format that can be extended and customized through the creation of new schemas. In the field of robotics, this format has received robust support and enhancements from NVIDIA Omniverse and its robotics extension, Isaac Sim, by integrating properties for the PhysX physics engine. Numerous parsers have been implemented to convert different formats into USD and vice versa, making USD a flexible and valuable format for describing complex scenes with photorealistic properties. Research efforts utilizing USD include studies that translate scene descriptions into knowledge graphs [235], the compilation of datasets containing real-world indoor scenes with annotated semantic segmentations [236], and the creation of neuro-symbolic representations of 3D scenes [237].

B. Learning physics-based attributes from videos

The choice of physics engine depends on the specific physical phenomena being modeled, as different engines offer varying features and support different physics parameters in their scene descriptions. Table V presents a brief comparison of simulators and their supported scene description formats. By selecting an appropriate simulator, one can encode the estimated physics parameters from an algorithm into the scene description and load them directly into the simulation environment.

For the rigid bodies aspect, object mass and friction can be estimated by aligning physics engine simulations with visual observations through methods like Markov Chain Monte Carlo (MCMC) [241]. Galileo [242] leverages this approach by using short MCMC runs to infer latent physical properties—such as mass, shape, and friction—based on how well the simulated outcomes match key features in video input. Additionally, the model incorporates deep learning to learn a direct mapping from visual data to physical parameters, effectively inverting part of the generative process for faster and more efficient inference. Another approach [243] estimates physical properties from video by combining a physics engine with a correction estimator. The system simulates object behavior from the initial state and refines parameters by comparing simulated and observed outcomes. It supports non-differentiable physics engines and uses either optimization techniques or neural networks for correction, showing robust performance in 2D bin scenarios.

In the context of soft body simulation, particularly cloth simulation, a deep learning-based approach [244] estimates cloth stiffness directly from video and applies it to virtual environments. This method leverages a Transformer architecture combined with pre-trained models such as ResNet50 [245] and VGG16 [246] to classify cloth behavior based on softness-to-stiffness labels. Trained on a dataset of 3840 videos, the model achieves an average accuracy of 99.5%, significantly outperforming traditional sequence models like RNNs, GRUs, and LSTMs. Another approach [247] passively estimates fabric stiffness and area weight by analyzing motion in videos under unknown wind forces. Using video texture features and a regression model, it accurately predicts material properties, validated against a ground truth dataset and human perceptual studies.

TABLE V
SIMULATORS COMPARISON TABLE

	Scene Description Formats		Outstanding features
	Main	Compatible	
MuJoCo [216]	MJCF	URDF	Fast and accurate physics for continuous control with smooth contact dynamics; great for reinforcement learning; used in research; Url: https://mujoco.org
Gazebo [217]	SDF	URDF	Modular and ROS-integrated; supports realistic sensor simulation; suitable for real-world robot prototyping; large plugin support; Url: https://gazebosim.org
PyBullet [218]	BULLET	SDF URDF MJCF	Easy scene prototyping with ML support; integrates OpenGL rendering for lightweight digital twin visualization; Url: https://pybullet.org
Webots [219]	PROTO	URDF	Fast setup of indoor environments with GUI and rich built-in robot/sensor models; User-friendly GUI; good for education; Url: https://cyberbotics.com
Drake [238]	MJCF	URDF	Analytical control modeling with structured dynamics; great for optimization in constrained spaces; Url: https://drake.mit.edu
SOFA [221]	SCN		Real-time soft-body simulation and surgical interaction modeling for indoor scenarios; Url: https://www.sofa-framework.org
Project Chrono [224]	JSON	URDF	Simulates rigid/flexible bodies, fluids, and granular materials; advanced multibody physics; Url: https://projectchrono.org
Omniverse [239]	USD	MJCF URDF	GPU-accelerated and photorealistic rendering; built for robotics digital twins with Isaac Sim; Url: https://www.nvidia.com/en-us/omniverse/
Unreal Engine	UASSET	USD	High visual fidelity, immersive VR/AR support, and accurate physics for indoor scene interaction; used for robotics, games, architecture; Url: https://www.unrealengine.com
Unity [226]	YAML		Fast-prototyping; cross-platform; ML and robotics integration via Unity Robotics Hub; Url: https://unity.com
Godot [240]	TSCN		Open-source and customizable; good for simple 3D/2D simulations; low resource use; Url: https://godotengine.org
Blender [227]	BLEND	USD	High-quality asset creation and scripting for synthetic data generation in robotics pipelines; large graphics community; Url: https://www.blender.org
Genesis [231]	USD	URDF MJCF	GPU-accelerated simulation with built-in generative tools for photorealistic indoor robotics datasets; Url: https://genesis-embodied-ai.github.io

In the context of fluid dynamics, viscosity is a key property that is typically measured using manual and time-consuming techniques. A recent method [248] employs 3D convolutional neural networks to estimate viscosity from videos of fluid motion recorded by a robotic system. By analyzing spatiotemporal patterns, the model predicts viscosity and fluid types with greater accuracy than human observers, supporting more efficient automated experimentation.

In summary, recent advances demonstrate that physical properties of rigid bodies, soft bodies, and fluids can be effectively estimated from visual data using a combination of simulation, optimization, and deep learning. These approaches enable automated and non-invasive inference of properties like mass, stiffness, and viscosity, supporting more accurate and efficient physical scene understanding across various domains.

C. Introducing physical properties in 3DGS representations

Various studies have utilized images and video data to drive generative dynamics using a 3D Gaussian approach. This method eliminates the need for traditional geometric constructs such as triangle/tetrahedron meshing, marching cubes, "cage meshes," or other forms of geometry embedding. A novel technique, PhysGaussian [249], has been developed to integrate physically grounded Newtonian dynamics within 3D Gaussians seamlessly, facilitating high-quality novel motion synthesis. This method uses a customized Material Point Method (MPM) that enhances 3D Gaussian kernels with physically significant kinematic deformation and mechanical

stress attributes, all governed by the principles of continuum mechanics. A key feature of this method is its smooth integration of physical simulation and visual rendering, where both components share the same 3D Gaussian kernels for their discrete representations.

This chapter explored the process of extracting physical properties from visual data to enable realistic and accurate physics-based simulations, which are essential for building digital twins. We reviewed widely used simulation engines across domains—rigid, soft, and fluid—and examined how their scene description formats influence integration and fidelity. Traditional formats like URDF offer basic support for rigid bodies but lack flexibility for complex dynamics, while newer formats like USD provide extensibility and support for photorealistic scenes. Advances in simulation, deep learning, and optimization now allow for the non-invasive estimation of physical parameters from video, making it possible to directly translate real-world observations into simulation-ready data. Emerging methods like 3D Gaussian representations further unify geometry, physics, and rendering into a compact, data-driven framework, pointing toward the future of simulation-based digital twin systems.

VI. DATASETS

A. Simultaneous Visualization of 3DGS and Mesh Models

The following options are capable of visualizing both **3D Gaussian Splatting (3DGS)** and traditional **mesh models** simultaneously:

- **1. NVIDIA Omniverse.** Supports USD format, allowing integration of both 3DGS (via custom rendering) and meshes. Compatible with NeRF-based techniques like Gaussian Splatting.
- **2. Blender (with Add-ons).** Blender’s shader nodes and geometry nodes can be used to load and render 3DGS data. Mesh rendering is natively supported. Requires a plugin like 3DGS Blender Addon (custom implementation might be necessary).
- **3. Unreal Engine (UE5).** Can handle 3D Gaussian Splatting via custom shaders or plugins. Natively supports mesh rendering.

B. Scene datasets

TABLE VI

SUMMARY OF DATA MODALITIES IN SELECTED SCENE DATASETS (X: AVAILABLE, O: PARTIAL)

Name	Type	RGB frames	Depth	Panorama	Mesh	Texture	Semantic segm.	Instance segm.	Articulated objects
Replica [250]	scan				x	x	x	x	
ReplicaCAD [251]	model				x	x	o	o	x
Matterport3D [252]	scan	x	x	x	x	x	x	x	
Matterport for Habitat	scan				x	x	o	o	
HSSD-200 [253]	model				x	x	x	x	
iThor dataset [254]	model				x	x	x	x	x
ProcTHOR [255]	model				x	x	x	x	x
Gibson Dataset [256]	scan	x			x	x	x		
3D-FRONT [257]	model				x	x	x	x	
ScanNet++ [258]	scan	x	x		x	x	x	x	

REFERENCES

- [1] T. Dai, J. Wong, Y. Jiang, C. Wang, C. Gokmen, R. Zhang, J. Wu, and L. Fei-Fei, “Automated creation of digital cousins for robust policy learning,” *arXiv preprint arXiv:2410.07408*, 2024.
- [2] A. P. S, A. Melnik, and G. C. Nandi, “Splatr : Experience goal visual rearrangement with 3d gaussian splatting and dense feature matching,” 2024. [Online]. Available: <https://arxiv.org/abs/2411.14322>
- [3] A. Melnik, L. Lach, M. Plappert, T. Korthals, R. Haschke, and H. Ritter, “Using tactile sensing to improve the sample efficiency and performance of deep deterministic policy gradients for simulated in-hand manipulation tasks,” *Frontiers in Robotics and AI*, vol. 8, p. 538773, 2021.
- [4] A. Melnik, M. Ljubljana, C. Lu, Q. Yan, W. Ren, and H. Ritter, “Video diffusion models: A survey,” *Transactions on Machine Learning Research*, 2024, survey Certification. [Online]. Available: <https://openreview.net/forum?id=rJSHjhEYJx>
- [5] A. Melnik, R. Schiewer, M. Lange, A. I. Muresanu, mozhgan saeidi, A. Garg, and H. Ritter, “Benchmarks for physical reasoning AI,” *Transactions on Machine Learning Research*, 2023, survey Certification. [Online]. Available: <https://openreview.net/forum?id=cHros8VIyN>
- [6] A. Melnik, F. Schüler, C. A. Rothkopf, and P. König, “The world as an external memory: The price of saccades in a sensorimotor task,” *Frontiers in behavioral neuroscience*, vol. 12, p. 253, 2018.
- [7] J. L. Schonberger and J.-M. Frahm, “Structure-from-motion revisited,” in *Proceedings of the IEEE conference on computer vision and pattern recognition*, 2016, pp. 4104–4113.
- [8] S. Ullman, “The interpretation of structure from motion,” *Proceedings of the Royal Society of London. Series B. Biological Sciences*, vol. 203, no. 1153, pp. 405–426, 1979.
- [9] D. G. Lowe, “Object recognition from local scale-invariant features,” in *Proceedings of the seventh IEEE international conference on computer vision*, vol. 2. Ieee, 1999, pp. 1150–1157.
- [10] P.-E. Sarlin, D. DeTone, T. Malisiewicz, and A. Rabinovich, “Superglue: Learning feature matching with graph neural networks,” in *Proceedings of the IEEE/CVF conference on computer vision and pattern recognition*, 2020, pp. 4938–4947.
- [11] J. Revaud, C. De Souza, M. Humenberger, and P. Weinzaepfel, “R2d2: Reliable and repeatable detector and descriptor,” *Advances in neural information processing systems*, vol. 32, 2019.
- [12] J. Sun, Z. Shen, Y. Wang, H. Bao, and X. Zhou, “Loftr: Detector-free local feature matching with transformers,” in *Proceedings of the IEEE/CVF conference on computer vision and pattern recognition*, 2021, pp. 8922–8931.
- [13] B. Triggs, P. F. McLauchlan, R. I. Hartley, and A. W. Fitzgibbon, “Bundle adjustment—a modern synthesis,” in *Vision Algorithms: Theory and Practice: International Workshop on Vision Algorithms Corfu, Greece, September 21–22, 1999 Proceedings*. Springer, 2000, pp. 298–372.
- [14] J. L. Schönberger, E. Zheng, J.-M. Frahm, and M. Pollefeys, “Pixelwise view selection for unstructured multi-view stereo,” in *Computer Vision—ECCV 2016: 14th European Conference, Amsterdam, The Netherlands, October 11–14, 2016, Proceedings, Part III 14*. Springer, 2016, pp. 501–518.
- [15] B. Kerbl, G. Kopanas, T. Leimkühler, and G. Drettakis, “3d gaussian splatting for real-time radiance field rendering,” *ACM Transactions on Graphics, volume 42(4)*, July 2023, Aug. 2023.
- [16] M. Rahman, H. Liu, M. Masri, I. Durazo-Cardenas, and A. Starr, “A railway track reconstruction method using robotic vision on a mobile manipulator: A proposed strategy,” *Computers in Industry*, vol. 148, p. 103900, 2023.
- [17] “3d gaussian splatting for real-time radiance field rendering,” <https://velog.io/@chahun1216/3D-Gaussian-Splatting-for-Real-Time-Radiance-Field-Rendering-%>

- EB%A6%AC%EB%B7%B0, last Accessed: 16/04/2025.
- [18] “A comprehensive overview of gaussian splatting,” <https://towardsdatascience.com/a-comprehensive-overview-of-gaussian-splatting-e7d57008346/>, last Accessed: 16/04/2025.
- [19] B. Huang, Z. Yu, A. Chen, A. Geiger, and S. Gao, “2d gaussian splatting for geometrically accurate radiance fields,” Mar. 2024.
- [20] Q.-Y. Zhou, S. Miller, and V. Koltun, “Elastic fragments for dense scene reconstruction,” in *Proceedings of the IEEE International Conference on Computer Vision*, 2013, pp. 473–480.
- [21] T. Schops, T. Sattler, and M. Pollefeys, “Bad slam: Bundle adjusted direct rgb-d slam,” in *Proceedings of the IEEE/CVF Conference on Computer Vision and Pattern Recognition*, 2019, pp. 134–144.
- [22] M. Nießner, M. Zollhöfer, S. Izadi, and M. Stamminger, “Real-time 3d reconstruction at scale using voxel hashing,” *ACM Transactions on Graphics (ToG)*, vol. 32, no. 6, pp. 1–11, 2013.
- [23] F. Steinbrucker, C. Kerl, and D. Cremers, “Large-scale multi-resolution surface reconstruction from rgb-d sequences,” in *Proceedings of the IEEE International Conference on Computer Vision*, 2013, pp. 3264–3271.
- [24] R. A. Newcombe, S. Izadi, O. Hilliges, D. Molyneaux, D. Kim, A. J. Davison, P. Kohi, J. Shotton, S. Hodges, and A. Fitzgibbon, “Kinectfusion: Real-time dense surface mapping and tracking,” in *2011 10th IEEE international symposium on mixed and augmented reality*. Ieee, 2011, pp. 127–136.
- [25] V. Yugay, Y. Li, T. Gevers, and M. R. Oswald, “Gaussian-slam: Photo-realistic dense slam with gaussian splatting,” Dec. 2023.
- [26] N. Keetha, J. Karhade, K. M. Jatavallabhula, G. Yang, S. Scherer, D. Ramanan, and J. Luiten, “Splatam: Splat, track & map 3d gaussians for dense rgb-d slam,” Dec. 2023.
- [27] C. Yan, D. Qu, D. Xu, B. Zhao, Z. Wang, D. Wang, and X. Li, “Gs-slam: Dense visual slam with 3d gaussian splatting,” nov 2023.
- [28] S. Sun, M. Mielle, A. J. Lilienthal, and M. Magnusson, “High-fidelity slam using gaussian splatting with rendering-guided densification and regularized optimization,” Mar. 2024.
- [29] S. Zhu, R. Qin, G. Wang, J. Liu, and H. Wang, “Semgauss-slam: Dense semantic gaussian splatting slam,” Mar. 2024.
- [30] K. Wang, C. Yang, Y. Wang, S. Li, Y. Wang, Q. Dou, X. Yang, and W. Shen, “Endogslam: Real-time dense reconstruction and tracking in endoscopic surgeries using gaussian splatting,” Mar. 2024.
- [31] L. C. Sun, N. P. Bhatt, J. C. Liu, Z. Fan, Z. Wang, T. E. Humphreys, and U. Topcu, “Mm3dgs slam: Multimodal 3d gaussian splatting for slam using vision, depth, and inertial measurements,” Apr. 2024.
- [32] T. Deng, Y. Chen, L. Zhang, J. Yang, S. Yuan, D. Wang, and W. Chen, “Compact 3d gaussian splatting for dense visual slam,” Mar. 2024.
- [33] Z. Peng, T. Shao, Y. Liu, J. Zhou, Y. Yang, J. Wang, and K. Zhou, “Rtg-slam: Real-time 3d reconstruction at scale using gaussian splatting,” Apr. 2024.
- [34] X. Hu, Y. Wang, L. Fan, J. Fan, J. Peng, Z. Lei, Q. Li, and Z. Zhang, “Sagd: Boundary-enhanced segment anything in 3d gaussian via gaussian decomposition,” Jan. 2024.
- [35] S. Ha, J. Yeon, and H. Yu, “Rgbd gs-icp slam,” Mar. 2024.
- [36] X. Zhou, X. Ran, Y. Xiong, J. He, Z. Lin, Y. Wang, D. Sun, and M.-H. Yang, “Gala3d: Towards text-to-3d complex scene generation via layout-guided generative gaussian splatting,” Feb. 2024.
- [37] Y. Ji, Y. Liu, G. Xie, B. Ma, and Z. Xie, “Neds-slam: A novel neural explicit dense semantic slam framework using 3d gaussian splatting,” Mar. 2024.
- [38] X. Lang, L. Li, H. Zhang, F. Xiong, M. Xu, Y. Liu, X. Zuo, and J. Lv, “Gaussian-lic: Photo-realistic lidar-inertial-camera slam with 3d gaussian splatting,” Apr. 2024.
- [39] M. Li, S. Liu, H. Zhou, G. Zhu, N. Cheng, T. Deng, and H. Wang, “Sgs-slam: Semantic gaussian splatting for neural dense slam,” Feb. 2024.
- [40] L. Zhu, Z. Wang, J. Cui, Z. Jin, G. Lin, and L. Yu, “Endogs: Deformable endoscopic tissues reconstruction with gaussian splatting,” Jan. 2024.
- [41] Y. Huang, B. Cui, L. Bai, Z. Guo, M. Xu, M. Islam, and H. Ren, “Endo-4dgs: Endoscopic monocular scene reconstruction with 4d gaussian splatting,” jan 2024.
- [42] M. Zwicker, H. Pfister, J. Van Baar, and M. Gross, “Ewa splatting,” *IEEE Transactions on Visualization and Computer Graphics*, vol. 8, no. 3, pp. 223–238, 2002.
- [43] S.-i. Amari, “Backpropagation and stochastic gradient descent method,” *Neurocomputing*, vol. 5, no. 4-5, pp. 185–196, 1993.
- [44] Z. Wang, A. C. Bovik, H. R. Sheikh, and E. P. Simoncelli, “Image quality assessment: from error visibility to structural similarity,” *IEEE transactions on image processing*, vol. 13, no. 4, pp. 600–612, 2004.
- [45] H. Pfister, M. Zwicker, J. van Baar, and M. Gross, “Surfels: surface elements as rendering primitives,” in *Proceedings of the 27th annual conference on Computer graphics and interactive techniques - SIGGRAPH '00*, ser. SIGGRAPH '00. ACM Press, 2000, pp. 335–342.
- [46] D. Chen, H. Li, W. Ye, Y. Wang, W. Xie, S. Zhai, N. Wang, H. Liu, H. Bao, and G. Zhang, “Pgsr: Planar-based gaussian splatting for efficient and high-fidelity surface reconstruction,” *IEEE Transactions on Visualization and Computer Graphics*, pp. 1–12, Jun. 2024.
- [47] P. Dai, J. Xu, W. Xie, X. Liu, H. Wang, and W. Xu, “High-quality surface reconstruction using gaussian surfels,” Apr. 2024.
- [48] X. Zhang, X. Ge, T. Xu, D. He, Y. Wang, H. Qin, G. Lu, J. Geng, and J. Zhang, “Gaussianimage: 1000 fps image representation and compression by 2d gaussian splatting,” Mar. 2024.

- [49] Y. Song, H. Lin, J. Lei, L. Liu, and K. Daniilidis, “Hdgs: Textured 2d gaussian splatting for enhanced scene rendering,” Dec. 2024.
- [50] S. Weiss and D. Bradley, “Gaussian billboards: Expressive 2d gaussian splatting with textures,” Dec. 2024.
- [51] H. Gao, R. Li, S. Tulsiani, B. Russell, and A. Kanazawa, “Monocular dynamic view synthesis: A reality check,” Oct. 2022.
- [52] H. Dahmani, M. Bennehar, N. Piasco, L. Roldao, and D. Tsishkou, “Swag: Splatting in the wild images with appearance-conditioned gaussians,” Mar. 2024.
- [53] T. Zhang, Q. Gao, W. Li, L. Liu, and B. Chen, “Bags: Building animatable gaussian splatting from a monocular video with diffusion priors,” Mar. 2024.
- [54] J. Oh, J. Chung, D. Lee, and K. M. Lee, “Deblurgs: Gaussian splatting for camera motion blur,” Apr. 2024.
- [55] L. Zhao, P. Wang, and P. Liu, “Bad-gaussians: Bundle adjusted deblur gaussian splatting,” Mar. 2024.
- [56] C. Peng, Y. Tang, Y. Zhou, N. Wang, X. Liu, D. Li, and R. Chellappa, “Bags: Blur agnostic gaussian splatting through multi-scale kernel modeling,” Mar. 2024.
- [57] O. Seiskari, J. Ylilammi, V. Kaatrasalo, P. Rantalankila, M. Turkulainen, J. Kannala, and A. Solin, “Gaussian splatting on the move: Blur and rolling shutter compensation for natural camera motion,” Mar. 2024.
- [58] Y. Fu, S. Liu, A. Kulkarni, J. Kautz, A. A. Efros, and X. Wang, “Colmap-free 3d gaussian splatting,” Dec. 2023.
- [59] C. Liu, S. Chen, Y. Bhalgat, S. Hu, M. Cheng, Z. Wang, V. A. Prisacariu, and T. Braud, “Gs-cpr: Efficient camera pose refinement via 3d gaussian splatting,” Aug. 2024.
- [60] Y. Sun, X. Wang, Y. Zhang, J. Zhang, C. Jiang, Y. Guo, and F. Wang, “icomma: Inverting 3d gaussian splatting for camera pose estimation via comparing and matching,” Dec. 2023.
- [61] G. Kang, J. Yoo, J. Park, S. Nam, S. Kim, H. Im, S. Shin, and E. Park, “Selfsplat: Pose-free and 3d prior-free generalizable 3d gaussian splatting,” Nov. 2024.
- [62] Z. Fan, J. Zhang, W. Cong, P. Wang, R. Li, K. Wen, S. Zhou, A. Kadambi, Z. Wang, D. Xu, B. Ivanovic, M. Pavone, and Y. Wang, “Large spatial model: End-to-end unposed images to semantic 3d,” Oct. 2024.
- [63] X. Cai, Y. Wang, Z. Fan, D. Haoran, S. Wang, W. Li, D. Li, L. Luo, M. Wang, and J. Xu, “Dust to tower: Coarse-to-fine photo-realistic scene reconstruction from sparse uncalibrated images,” Dec. 2024.
- [64] Y. Chen, R. A. Potamias, E. Ververas, J. Song, J. Deng, and G. H. Lee, “Zerogs: Training 3d gaussian splatting from unposed images,” Nov. 2024.
- [65] D. Shi, S. Cao, L. Fan, B. Wu, J. Guo, R. Chen, L. Liu, and J. Ye, “Trackgs: Optimizing colmap-free 3d gaussian splatting with global track constraints,” Feb. 2025.
- [66] H. Li, Y. Gao, C. Wu, D. Zhang, Y. Dai, C. Zhao, H. Feng, E. Ding, J. Wang, and J. Han, “Ggrt: Towards pose-free generalizable 3d gaussian splatting in real-time,” Mar. 2024.
- [67] Y. Deng, W. Xian, G. Yang, L. Guibas, G. Wetzstein, S. Marschner, and P. Debevec, “Self-calibrating gaussian splatting for large field of view reconstruction,” *arXiv preprint arXiv:2502.09563*, 2025.
- [68] J. Behrmann, W. Grathwohl, R. T. Chen, D. Duvenaud, and J.-H. Jacobsen, “Invertible residual networks,” in *International conference on machine learning*. PMLR, 2019, pp. 573–582.
- [69] E. T. Jonasson, L. R. Pinto, and A. Vale, “Comparison of three key remote sensing technologies for mobile robot localization in nuclear facilities,” *Fusion Engineering and Design*, vol. 172, p. 112691, 2021.
- [70] J. Tang, J. Ren, H. Zhou, Z. Liu, and G. Zeng, “Dream-gaussian: Generative gaussian splatting for efficient 3d content creation,” Sep. 2023.
- [71] T. Yi, J. Fang, J. Wang, G. Wu, L. Xie, X. Zhang, W. Liu, Q. Tian, and X. Wang, “Gaussiandreamer: Fast generation from text to 3d gaussians by bridging 2d and 3d diffusion models,” oct 2023.
- [72] Q. Feng, Z. Xing, Z. Wu, and Y.-G. Jiang, “Fdgaussian: Fast gaussian splatting from single image via geometric-aware diffusion model,” Mar. 2024.
- [73] X. He, J. Chen, S. Peng, D. Huang, Y. Li, X. Huang, C. Yuan, W. Ouyang, and T. He, “Gvgen: Text-to-3d generation with volumetric representation,” Mar. 2024.
- [74] L. Jiang and L. Wang, “Brightdreamer: Generic 3d gaussian generative framework for fast text-to-3d synthesis,” Mar. 2024.
- [75] Y. Lin, R. Clark, and P. Torr, “Dreampolisher: Towards high-quality text-to-3d generation via geometric diffusion,” Mar. 2024.
- [76] D. Di, J. Yang, C. Luo, Z. Xue, W. Chen, X. Yang, and Y. Gao, “Hyper-3dg: Text-to-3d gaussian generation via hypergraph,” Mar. 2024.
- [77] J. Tang, Z. Chen, X. Chen, T. Wang, G. Zeng, and Z. Liu, “Lgm: Large multi-view gaussian model for high-resolution 3d content creation,” Feb. 2024.
- [78] L. Melas-Kyriazi, I. Laina, C. Rupprecht, N. Neverova, A. Vedaldi, O. Gafni, and F. Kokkinos, “Im-3d: Iterative multiview diffusion and reconstruction for high-quality 3d generation,” Feb. 2024.
- [79] J. Chung, S. Lee, H. Nam, J. Lee, and K. M. Lee, “Luciddreamer: Domain-free generation of 3d gaussian splatting scenes,” nov 2023.
- [80] H. Li, H. Shi, W. Zhang, W. Wu, Y. Liao, L. Wang, L.-h. Lee, and P. Zhou, “Dreamscene: 3d gaussian-based text-to-3d scene generation via formation pattern sampling,” Apr. 2024.
- [81] J. Shriram, A. Trevithick, L. Liu, and R. Ramamoorthi, “Realdreamer: Text-driven 3d scene generation with inpainting and depth diffusion,” Apr. 2024.
- [82] S. Zhou, Z. Fan, D. Xu, H. Chang, P. Chari, T. Bhargava, S. You, Z. Wang, and A. Kadambi, “Dreamscene360: Unconstrained text-to-3d scene generation with panoramic gaussian splatting,” Apr. 2024.
- [83] Y. Yin, D. Xu, Z. Wang, Y. Zhao, and Y. Wei, “4dgen: Grounded 4d content generation with spatial-temporal consistency,” dec 2023.

- [84] J. Ren, L. Pan, J. Tang, C. Zhang, A. Cao, G. Zeng, and Z. Liu, “Dreamgaussian4d: Generative 4d gaussian splatting,” Dec. 2023.
- [85] Z. Pan, Z. Yang, X. Zhu, and L. Zhang, “Fast dynamic 3d object generation from a single-view video,” Jan. 2024.
- [86] Y. Wang, X. Wang, Z. Chen, Z. Wang, F. Sun, and J. Zhu, “Vidu4d: Single generated video to high-fidelity 4d reconstruction with dynamic gaussian surfels,” may 2024.
- [87] Z. Wu, C. Yu, Y. Jiang, C. Cao, F. Wang, and X. Bai, “Sc4d: Sparse-controlled video-to-4d generation and motion transfer,” *arxiv:2404.03736*, Apr. 2024.
- [88] Y. Zeng, Y. Jiang, S. Zhu, Y. Lu, Y. Lin, H. Zhu, W. Hu, X. Cao, and Y. Yao, “Stag4d: Spatial-temporal anchored generative 4d gaussians,” Mar. 2024.
- [89] T. Alldieck, N. Kolotouros, and C. Sminchisescu, “Score distillation sampling with learned manifold corrective,” in *European Conference on Computer Vision*. Springer, 2024, pp. 1–18.
- [90] B. Zhang, Y. Cheng, J. Yang, C. Wang, F. Zhao, Y. Tang, D. Chen, and B. Guo, “Gaussiancube: A structured and explicit radiance representation for 3d generative modeling,” Mar. 2024.
- [91] Z. Yang, X. Gao, W. Zhou, S. Jiao, Y. Zhang, and X. Jin, “Deformable 3d gaussians for high-fidelity monocular dynamic scene reconstruction,” in *Proceedings of the IEEE/CVF Conference on Computer Vision and Pattern Recognition (CVPR)*, June 2024, pp. 20 331–20 341.
- [92] D. Xu, H. Liang, N. P. Bhatt, H. Hu, H. Liang, K. N. Plataniotis, and Z. Wang, “Comp4d: Llm-guided compositional 4d scene generation,” Mar. 2024.
- [93] D. Xu, Y. Yuan, M. Mardani, S. Liu, J. Song, Z. Wang, and A. Vahdat, “Agg: Amortized generative 3d gaussians for single image to 3d,” Jan. 2024.
- [94] X. Yang and X. Wang, “Hash3d: Training-free acceleration for 3d generation,” Apr. 2024.
- [95] P. Jiang, G. Pandey, and S. Saripalli, “3dgs-reloc: 3d gaussian splatting for map representation and visual relocalization,” Mar. 2024.
- [96] A. Melnik, M. Miasayedzenkau, D. Makaravets, D. Pirshtuk, E. Akbulut, D. Holzmann, T. Rensch, G. Reichert, and H. Ritter, “Face generation and editing with stylegan: A survey,” *IEEE Transactions on pattern analysis and machine intelligence*, vol. 46, no. 5, pp. 3557–3576, 2024.
- [97] Z. Li, Y. Chen, L. Zhao, and P. Liu, “Controllable text-to-3d generation via surface-aligned gaussian splatting,” Mar. 2024.
- [98] Y. Nie, X. Han, S. Guo, Y. Zheng, J. Chang, and J. J. Zhang, “Total3DUnderstanding: Joint layout, object pose and mesh reconstruction for indoor scenes from a single image,” in *Proceedings of the IEEE/CVF Conference on Computer Vision and Pattern Recognition*, 2020, pp. 55–64.
- [99] C. Zhang, Z. Cui, Y. Zhang, B. Zeng, M. Pollefeys, and S. Liu, “Holistic 3D scene understanding from a single image with implicit representation,” in *Proceedings of the IEEE/CVF Conference on Computer Vision and Pattern Recognition*, 2021, pp. 8833–8842.
- [100] G. Gkioxari, N. Ravi, and J. Johnson, “Learning 3d object shape and layout without 3d supervision,” in *Proceedings of the IEEE/CVF Conference on Computer Vision and Pattern Recognition*, 2022, pp. 1695–1704.
- [101] H. Liu, Y. Zheng, G. Chen, S. Cui, and X. Han, “Towards high-fidelity single-view holistic reconstruction of indoor scenes,” in *European Conference on Computer Vision*. Springer, 2022, pp. 429–446.
- [102] X. Zhang, Z. Chen, F. Wei, and Z. Tu, “Uni-3d: A universal model for panoptic 3d scene reconstruction,” in *Proceedings of the IEEE/CVF International Conference on Computer Vision*, 2023, pp. 9256–9266.
- [103] Y. Chen, J. Ni, N. Jiang, Y. Zhang, Y. Zhu, and S. Huang, “Single-view 3D scene reconstruction with high-fidelity shape and texture,” in *2024 International Conference on 3D Vision (3DV)*. IEEE, 2024, pp. 1456–1467.
- [104] A. Dogaru, M. Özer, and B. Egger, “Generalizable 3d scene reconstruction via divide and conquer from a single view,” *arXiv preprint arXiv:2404.03421*, 2024.
- [105] Z. Huang, Y.-C. Guo, X. An, Y. Yang, Y. Li, Z.-X. Zou, D. Liang, X. Liu, Y.-P. Cao, and L. Sheng, “Midi: Multi-instance diffusion for single image to 3d scene generation,” *arXiv preprint arXiv:2412.03558*, 2024.
- [106] J. Zhou, Y.-S. Liu, and Z. Han, “Zero-shot scene reconstruction from single images with deep prior assembly,” *arXiv preprint arXiv:2410.15971*, 2024.
- [107] M. Dahnert, A. Dai, N. Müller, and M. Nießner, “Coherent 3d scene diffusion from a single rgb image,” *Advances in Neural Information Processing Systems*, vol. 37, pp. 23 435–23 463, 2024.
- [108] K. Yao, L. Zhang, X. Yan, Y. Zeng, Q. Zhang, L. Xu, W. Yang, J. Gu, and J. Yu, “Cast: Component-aligned 3d scene reconstruction from an rgb image,” *arXiv preprint arXiv:2502.12894*, 2025.
- [109] H. Izadinia, Q. Shan, and S. M. Seitz, “IM2CAD,” in *CVPR*, 2017, pp. 5134–5143.
- [110] W. Kuo, A. Angelova, T.-Y. Lin, and A. Dai, “Mask2CAD: 3D shape prediction by learning to segment and retrieve,” in *ECCV*, vol. 1. Springer, 2020, p. 3.
- [111] —, “Patch2CAD: Patchwise embedding learning for in-the-wild shape retrieval from a single image,” in *ICCV*, 2021, pp. 12 589–12 599.
- [112] C. Gümeli, A. Dai, and M. Nießner, “ROCA: robust CAD model retrieval and alignment from a single image,” in *CVPR*, 2022, pp. 4022–4031.
- [113] K. Yan, F. Luan, M. Hašan, T. Groueix, V. Deschaintre, and S. Zhao, “Psdr-room: Single photo to scene using differentiable rendering,” in *SIGGRAPH Asia 2023 Conference Papers*, 2023, pp. 1–11.
- [114] D. Gao, D. Rozenberszki, S. Leutenegger, and A. Dai, “DiffCAD: Weakly-supervised probabilistic CAD model retrieval and alignment from an RGB image,” *ACM Transactions on Graphics (TOG)*, vol. 43, no. 4, pp. 1–15, 2024.

- [115] Q. Wu, D. Iliash, D. Ritchie, M. Savva, and A. X. Chang, “Diorama: Unleashing zero-shot single-view 3d scene modeling,” *arXiv preprint arXiv:2411.19492*, 2024.
- [116] A. Paliwal, W. Ye, J. Xiong, D. Kotovenko, R. Ranjan, V. Chandra, and N. K. Kalantari, “Coherentgs: Sparse novel view synthesis with coherent 3d gaussians,” Mar. 2024.
- [117] C. Yang, S. Li, J. Fang, R. Liang, L. Xie, X. Zhang, W. Shen, and Q. Tian, “Gaussianobject: Just taking four images to get a high-quality 3d object with gaussian splatting,” Feb. 2024.
- [118] Q. Shen, Z. Wu, X. Yi, P. Zhou, H. Zhang, S. Yan, and X. Wang, “Gamba: Marry gaussian splatting with mamba for single view 3d reconstruction,” Mar. 2024.
- [119] Y. Xu, Z. Shi, W. Yifan, H. Chen, C. Yang, S. Peng, Y. Shen, and G. Wetzstein, “Grm: Large gaussian reconstruction model for efficient 3d reconstruction and generation,” Mar. 2024.
- [120] S. Szymanowicz, C. Rupprecht, and A. Vedaldi, “Splatter image: Ultra-fast single-view 3d reconstruction,” Dec. 2023.
- [121] J. Zhang, Z. Tang, Y. Pang, X. Cheng, P. Jin, Y. Wei, M. Ning, and L. Yuan, “Repaint123: Fast and high-quality one image to 3d generation with progressive controllable 2d repainting,” Dec. 2023.
- [122] J. Wu, J.-W. Bian, X. Li, G. Wang, I. Reid, P. Torr, and V. A. Prisacariu, “Gaussctrl: Multi-view consistent text-driven 3d gaussian splatting editing,” Mar. 2024.
- [123] Y. Chen, Z. Chen, C. Zhang, F. Wang, X. Yang, Y. Wang, Z. Cai, L. Yang, H. Liu, and G. Lin, “Gaussianeditor: Swift and controllable 3d editing with gaussian splatting,” nov 2023.
- [124] Y. Chen, T. He, D. Huang, W. Ye, S. Chen, J. Tang, X. Chen, Z. Cai, L. Yang, G. Yu *et al.*, “Meshanything: Artist-created mesh generation with autoregressive transformers,” *arXiv preprint arXiv:2406.10163*, 2024.
- [125] B. Kerbl, G. Kopanas, T. Leimkühler, and G. Drettakis, “3d gaussian splatting for real-time radiance field rendering,” *ACM Trans. Graph.*, vol. 42, no. 4, pp. 139–1, 2023.
- [126] A. Guédon and V. Lepetit, “Sugar: Surface-aligned gaussian splatting for efficient 3d mesh reconstruction and high-quality mesh rendering,” Nov. 2023.
- [127] Z. Fan, K. Wen, W. Cong, K. Wang, J. Zhang, X. Ding, D. Xu, B. Ivanovic, M. Pavone, G. Pavlakos, Z. Wang, and Y. Wang, “Instantsplat: Sparse-view sfm-free gaussian splatting in seconds,” 2024. [Online]. Available: <https://arxiv.org/abs/2403.20309>
- [128] S. Wang, V. Leroy, Y. Cabon, B. Chidlovskii, and J. Revaud, “Dust3r: Geometric 3d vision made easy,” in *Proceedings of the IEEE/CVF Conference on Computer Vision and Pattern Recognition*, 2024, pp. 20 697–20 709.
- [129] V. Leroy, Y. Cabon, and J. Revaud, “Grounding image matching in 3d with mast3r,” in *European Conference on Computer Vision*. Springer, 2024, pp. 71–91.
- [130] L. Yang, B. Kang, Z. Huang, Z. Zhao, X. Xu, J. Feng, and H. Zhao, “Depth anything v2,” *Advances in Neural Information Processing Systems*, vol. 37, pp. 21 875–21 911, 2025.
- [131] A. Melnik, M. Büttner, L. Harz, L. Brown, G. C. Nandi, A. PS, G. K. Yadav, R. Kala, and R. Haschke, “Uniteam: Open vocabulary mobile manipulation challenge,” *arXiv preprint arXiv:2312.08611*, 2023.
- [132] S. Yenamandra, A. Ramachandran, M. Khanna, K. Yadav, J. Vakil, A. Melnik, M. Büttner, L. Harz, L. Brown, G. C. Nandi *et al.*, “Towards open-world mobile manipulation in homes: Lessons from the neurips 2023 home-robot open vocabulary mobile manipulation challenge,” *arXiv preprint arXiv:2407.06939*, 2024.
- [133] C. Li, R. Zhang, J. Wong, C. Gokmen, S. Srivastava, R. Martín-Martín, C. Wang, G. Levine, M. Lingelbach, J. Sun, M. Anvari, M. Hwang, M. Sharma, A. Aydin, D. Bansal, S. Hunter, K.-Y. Kim, A. Lou, C. R. Matthews, I. Villa-Renteria, J. H. Tang, C. Tang, F. Xia, S. Savarese, H. Gweon, K. Liu, J. Wu, and L. Fei-Fei, “BEHAVIOR-1k: A benchmark for embodied AI with 1,000 everyday activities and realistic simulation,” in *6th Annual Conference on Robot Learning*, 2022. [Online]. Available: https://openreview.net/forum?id=_8DoIe8G3t
- [134] J. Liu, D. Iliash, A. X. Chang, M. Savva, and A. Mahdavi-Amiri, “Singapo: Single image controlled generation of articulated parts in objects,” *arXiv preprint arXiv:2410.16499*, 2024.
- [135] D. Gao, D. Rozenberszki, S. Leutenegger, and A. Dai, “Diffcad: Weakly-supervised probabilistic cad model retrieval and alignment from an rgb image,” *ACM Transactions on Graphics (TOG)*, vol. 43, no. 4, pp. 1–15, 2024.
- [136] A. Melnik, A. Harter, C. Limberg, K. Rana, N. Sünderhauf, and H. Ritter, “Critic guided segmentation of rewarding objects in first-person views,” in *KI 2021: Advances in Artificial Intelligence: 44th German Conference on AI, Virtual Event, September 27–October 1, 2021, Proceedings 44*. Springer, 2021, pp. 338–348.
- [137] M. Oquab, T. Darcet, T. Moutakanni, H. Vo, M. Szafraniec, V. Khalidov, P. Fernandez, D. Haziza, F. Massa, A. El-Nouby *et al.*, “Dinov2: Learning robust visual features without supervision,” *arXiv preprint arXiv:2304.07193*, 2023.
- [138] H.-H. Lee, Y. Zhang, and A. X. Chang, “Duoduo clip: Efficient 3d understanding with multi-view images,” 2024.
- [139] Q. Wu, D. Ritchie, M. Savva, and A. X. Chang, “Generalizing single-view 3d shape retrieval to occlusions and unseen objects,” in *2024 International Conference on 3D Vision (3DV)*. IEEE, 2024, pp. 893–902.
- [140] D.-Y. Chen, X.-P. Tian, Y.-T. Shen, and M. Ouhyoung, “On visual similarity based 3D model retrieval,” *CGF*, vol. 22, no. 3, pp. 223–232, 2003.
- [141] M.-X. Lin, J. Yang, H. Wang, Y.-K. Lai, R. Jia, B. Zhao, and L. Gao, “Single image 3D shape retrieval via cross-modal instance and category contrastive learning,” in

- ICCV, 2021, pp. 11405–11415.
- [142] M. Rothgänger, A. Melnik, and H. Ritter, “Shape complexity estimation using vae,” in *Intelligent Systems Conference*. Springer, 2023, pp. 35–45.
- [143] K. Chen, C. B. Choy, M. Savva, A. X. Chang, T. Funkhouser, and S. Savarese, “Text2shape: Generating shapes from natural language by learning joint embeddings,” in *Computer Vision—ACCV 2018: 14th Asian Conference on Computer Vision, Perth, Australia, December 2–6, 2018, Revised Selected Papers, Part III 14*. Springer, 2019, pp. 100–116.
- [144] Y. Ruan, H.-H. Lee, Y. Zhang, K. Zhang, and A. X. Chang, “Tricolo: Trimodal contrastive loss for text to shape retrieval,” in *Proceedings of the IEEE/CVF Winter Conference on Applications of Computer Vision*, 2024, pp. 5815–5825.
- [145] F. Langer, J. Ju, G. Dikov, G. Reitmayr, and M. Ghafoorian, “FastCAD: Real-time CAD retrieval and alignment from scans and videos,” *arXiv preprint arXiv:2403.15161*, 2024.
- [146] X. He, Y. Zhou, Z. Zhou, S. Bai, and X. Bai, “Triplet-center loss for multi-view 3D object retrieval,” in *CVPR*, 2018, pp. 1945–1954.
- [147] H. Fu, S. Li, R. Jia, M. Gong, B. Zhao, and D. Tao, “Hard example generation by texture synthesis for cross-domain shape similarity learning,” *NeurIPS*, vol. 33, pp. 14675–14687, 2020.
- [148] M. A. Uy, V. G. Kim, M. Sung, N. Aigerman, S. Chaudhuri, and L. J. Guibas, “Joint learning of 3D shape retrieval and deformation,” in *CVPR*, 2021, pp. 11713–11722.
- [149] A. Radford, J. W. Kim, C. Hallacy, A. Ramesh, G. Goh, S. Agarwal, G. Sastry, A. Askell, P. Mishkin, J. Clark *et al.*, “Learning transferable visual models from natural language supervision,” in *International conference on machine learning*. PMLR, 2021, pp. 8748–8763.
- [150] L. Xue, M. Gao, C. Xing, R. Martín-Martín, J. Wu, C. Xiong, R. Xu, J. C. Niebles, and S. Savarese, “Ulip: Learning unified representation of language, image and point cloud for 3d understanding,” *arXiv preprint arXiv:2212.05171*, 2022.
- [151] M. Liu, R. Shi, K. Kuang, Y. Zhu, X. Li, S. Han, H. Cai, F. Porikli, and H. Su, “Openshape: Scaling up 3d shape representation towards open-world understanding,” 2023.
- [152] L. Xue, N. Yu, S. Zhang, J. Li, R. Martín-Martín, J. Wu, C. Xiong, R. Xu, J. C. Niebles, and S. Savarese, “Ulip-2: Towards scalable multimodal pre-training for 3d understanding,” 2023.
- [153] A. X. Chang, T. Funkhouser, L. Guibas, P. Hanrahan, Q. Huang, Z. Li, S. Savarese, M. Savva, S. Song, H. Su *et al.*, “Shapenet: An information-rich 3d model repository,” *arXiv preprint arXiv:1512.03012*, 2015.
- [154] M. Deitke, D. Schwenk, J. Salvador, L. Weihs, O. Michel, E. VanderBilt, L. Schmidt, K. Ehsani, A. Kembhavi, and A. Farhadi, “Objaverse: A universe of annotated 3d objects,” *arXiv preprint arXiv:2212.08051*, 2022.
- [155] J. Zhou, J. Wang, B. Ma, Y.-S. Liu, T. Huang, and X. Wang, “Uni3d: Exploring unified 3d representation at scale,” in *International Conference on Learning Representations (ICLR)*, 2024.
- [156] K. Ye, Q. Hou, and K. Zhou, “3D Gaussian Splatting with Deferred Reflection,” in *Special Interest Group on Computer Graphics and Interactive Techniques Conference Conference Papers '24*. Denver CO USA: ACM, Jul. 2024. [Online]. Available: <https://dl.acm.org/doi/10.1145/3641519.3657456>
- [157] J. Gao, C. Gu, Y. Lin, H. Zhu, X. Cao, L. Zhang, and Y. Yao, “Relightable 3d gaussian: Real-time point cloud relighting with brdf decomposition and ray tracing,” *arXiv:2311.16043*, 2023.
- [158] Z. Liang, Q. Zhang, Y. Feng, Y. Shan, and K. Jia, “Gs-ir: 3d gaussian splatting for inverse rendering,” *arXiv preprint arXiv:2311.16473*, 2023.
- [159] Y. Jiang, J. Tu, Y. Liu, X. Gao, X. Long, W. Wang, and Y. Ma, “Gaussianshader: 3d gaussian splatting with shading functions for reflective surfaces,” *arXiv preprint arXiv:2311.17977*, 2023.
- [160] Y. Shi, Y. Wu, C. Wu, X. Liu, C. Zhao, H. Feng, J. Zhang, B. Zhou, E. Ding, and J. Wang, “Gir: 3d gaussian inverse rendering for relightable scene factorization,” *arXiv preprint arXiv:2312.05133*, 2023.
- [161] T. Wu, J.-M. Sun, Y.-K. Lai, Y. Ma, L. Kobbelt, and L. Gao, “Deferredgds: Decoupled and editable gaussian splatting with deferred shading,” 2024. [Online]. Available: <https://arxiv.org/abs/2404.09412>
- [162] H. Chen, Z. Lin, and J. Zhang, “Gi-gs: Global illumination decomposition on gaussian splatting for inverse rendering,” 2024. [Online]. Available: <https://arxiv.org/abs/2410.02619>
- [163] Z. Bi, Y. Zeng, C. Zeng, F. Pei, X. Feng, K. Zhou, and H. Wu, “Gs³: Efficient relighting with triple gaussian splatting,” in *SIGGRAPH Asia 2024 Conference Papers*, 2024.
- [164] B. Huang, Z. Yu, A. Chen, A. Geiger, and S. Gao, “2d gaussian splatting for geometrically accurate radiance fields,” in *Special Interest Group on Computer Graphics and Interactive Techniques Conference Conference Papers '24*, ser. SIGGRAPH '24. ACM, Jul. 2024, p. 1–11. [Online]. Available: <http://dx.doi.org/10.1145/3641519.3657428>
- [165] K. Du, Z. Liang, and Z. Wang, “Gs-id: Illumination decomposition on gaussian splatting via diffusion prior and parametric light source optimization,” 2024. [Online]. Available: <https://arxiv.org/abs/2408.08524>
- [166] Y. Yao, Z. Zeng, C. Gu, X. Zhu, and L. Zhang, “Reflective gaussian splatting,” 2025. [Online]. Available: <https://arxiv.org/abs/2412.19282>
- [167] J. Li, Z. Wu, E. Zamfir, and R. Timofte, “Recap: Better gaussian relighting with cross-environment captures,” 2024. [Online]. Available: <https://arxiv.org/abs/2412.07534>
- [168] J. Fan, F. Luan, J. Yang, M. Hašan, and B. Wang, “Rng: Relightable neural gaussians,” 2024. [Online]. Available: <https://arxiv.org/abs/2409.19702>

- [169] J. Liu, X. Tang, F. Cheng, R. Yang, Z. Li, J. Liu, Y. Huang, J. Lin, S. Liu, X. Wu, S. Xu, and C. Yuan, "Mirrorgaussian: Reflecting 3d gaussians for reconstructing mirror reflections," in *Computer Vision – ECCV 2024*. Cham: Springer Nature Switzerland, 2025, pp. 377–393.
- [170] J. Meng, H. Li, Y. Wu, Q. Gao, S. Yang, J. Zhang, and S. Ma, "Mirror-3dgs: Incorporating mirror reflections into 3d gaussian splatting," in *2024 IEEE International Conference on Visual Communications and Image Processing (VCIP)*, 2024, pp. 1–5.
- [171] Z. Wang, S. Wang, M. Turkulainen, J. Fang, and J. Kannala, "Gaussian splatting in mirrors: Reflection-aware rendering via virtual camera optimization," *arXiv preprint arXiv:2410.01614*, 2024.
- [172] A. Kirillov, E. Mintun, N. Ravi, H. Mao, C. Rolland, L. Gustafson, T. Xiao, S. Whitehead, A. C. Berg, W.-Y. Lo *et al.*, "Segment anything," in *Proceedings of the IEEE/CVF international conference on computer vision*, 2023, pp. 4015–4026.
- [173] J. Cao, J. Cui, and S. Schwertfeger, "GlassGaussian: Extending 3D Gaussian Splatting for Realistic Imperfections and Glass Materials," *IEEE Access*, vol. 13, pp. 31 517–31 531, 2025. [Online]. Available: <https://ieeexplore.ieee.org/document/10884729>
- [174] R. Zhang, T. Luo, W. Yang, B. Fei, J. Xu, Q. Zhou, K. Liu, and Y. He, "Refgaussian: Disentangling reflections from 3d gaussian splatting for realistic rendering," *arXiv preprint arXiv:2406.05852*, 2024.
- [175] Z. Wang, Z. Li, Z. Tang, Y. Hao, and H. He, "Space-view decoupled 3d gaussians for novel-view synthesis of mirror reflections," in *Pacific Rim International Conference on Artificial Intelligence*. Springer, 2024, pp. 76–88.
- [176] T. Li, M. Slavcheva, M. Zollhöfer, S. Green, C. Lassner, C. Kim, T. Schmidt, S. Lovegrove, M. Goesele, R. Newcombe, and Z. Lv, "Neural 3d video synthesis from multi-view video," in *Proceedings of the IEEE/CVF Conference on Computer Vision and Pattern Recognition (CVPR)*, June 2022, pp. 5521–5531.
- [177] F. Wang, S. Tan, X. Li, Z. Tian, Y. Song, and H. Liu, "Mixed neural voxels for fast multi-view video synthesis," in *Proceedings of the IEEE/CVF International Conference on Computer Vision (ICCV)*, October 2023, pp. 19 706–19 716.
- [178] S. Fridovich-Keil, G. Meanti, F. R. Warburg, B. Recht, and A. Kanazawa, "K-planes: Explicit radiance fields in space, time, and appearance," in *Proceedings of the IEEE/CVF Conference on Computer Vision and Pattern Recognition (CVPR)*, June 2023, pp. 12 479–12 488.
- [179] Y. Liang, N. Khan, Z. Li, T. Nguyen-Phuoc, D. Lanman, J. Tompkin, and L. Xiao, "GauFR: Gaussian Deformation Fields for Real-Time Dynamic Novel View Synthesis," in *2025 IEEE/CVF Winter Conference on Applications of Computer Vision (WACV)*. Los Alamitos, CA, USA: IEEE Computer Society, Mar. 2025, pp. 2642–2652. [Online]. Available: <https://doi.ieeecomputersociety.org/10.1109/WACV61041.2025.00262>
- [180] A. Pumarola, E. Corona, G. Pons-Moll, and F. Moreno-Noguer, "D-nerf: Neural radiance fields for dynamic scenes," in *Proceedings of the IEEE/CVF Conference on Computer Vision and Pattern Recognition (CVPR)*, June 2021, pp. 10 318–10 327.
- [181] J. Fang, T. Yi, X. Wang, L. Xie, X. Zhang, W. Liu, M. Nießner, and Q. Tian, "Fast dynamic radiance fields with time-aware neural voxels," in *SIGGRAPH Asia 2022 Conference Papers*, ser. SA '22. New York, NY, USA: Association for Computing Machinery, 2022. [Online]. Available: <https://doi.org/10.1145/3550469.3555383>
- [182] W. Gan, H. Xu, Y. Huang, S. Chen, and N. Yokoya, "V4d: Voxel for 4d novel view synthesis," *IEEE Transactions on Visualization and Computer Graphics*, vol. 30, no. 2, pp. 1579–1591, 2024.
- [183] A. Cao and J. Johnson, "Hexplane: A fast representation for dynamic scenes," in *Proceedings of the IEEE/CVF Conference on Computer Vision and Pattern Recognition (CVPR)*, June 2023, pp. 130–141.
- [184] Z. Xu, S. Peng, H. Lin, G. He, J. Sun, Y. Shen, H. Bao, and X. Zhou, "4k4d: Real-time 4d view synthesis at 4k resolution," in *2024 IEEE/CVF Conference on Computer Vision and Pattern Recognition (CVPR)*, 2024, pp. 20 029–20 040.
- [185] G. Wu, T. Yi, J. Fang, L. Xie, X. Zhang, W. Wei, W. Liu, Q. Tian, and X. Wang, "4d gaussian splatting for real-time dynamic scene rendering," in *Proceedings of the IEEE/CVF Conference on Computer Vision and Pattern Recognition (CVPR)*, June 2024, pp. 20 310–20 320.
- [186] Z. Li, Z. Chen, Z. Li, and Y. Xu, "Spacetime gaussian feature splatting for real-time dynamic view synthesis," in *Proceedings of the IEEE/CVF Conference on Computer Vision and Pattern Recognition (CVPR)*, June 2024, pp. 8508–8520.
- [187] J. Luiten, G. Kopanas, B. Leibe, and D. Ramanan, "Dynamic 3d gaussians: Tracking by persistent dynamic view synthesis," in *2024 International Conference on 3D Vision (3DV)*, 2024, pp. 800–809.
- [188] Z. Yang, H. Yang, Z. Pan, and L. Zhang, "Real-time photorealistic dynamic scene representation and rendering with 4d gaussian splatting," in *International Conference on Learning Representations (ICLR)*, 2024.
- [189] A. Kratimenos, J. Lei, and K. Daniilidis, "Dyngm: Neural motion factorization for real-time dynamic view synthesis with 3d gaussian splatting," *ECCV*, 2024.
- [190] Y.-H. Huang, Y.-T. Sun, Z. Yang, X. Lyu, Y.-P. Cao, and X. Qi, "Sc-gs: Sparse-controlled gaussian splatting for editable dynamic scenes," in *Proceedings of the IEEE/CVF Conference on Computer Vision and Pattern Recognition (CVPR)*, June 2024, pp. 4220–4230.
- [191] Z. Yan, R. Hu, X. Yan, L. Chen, O. Van Kaick, H. Zhang, and H. Huang, "Rpm-net: recurrent prediction of motion and parts from point cloud," *arXiv preprint arXiv:2006.14865*, 2020.
- [192] X. Wang, B. Zhou, Y. Shi, X. Chen, Q. Zhao, and K. Xu, "Shape2motion: Joint analysis of motion parts

- and attributes from 3d shapes,” in *Proceedings of the IEEE/CVF Conference on Computer Vision and Pattern Recognition*, 2019, pp. 8876–8884.
- [193] F. Xiang, Y. Qin, K. Mo, Y. Xia, H. Zhu, F. Liu, M. Liu, H. Jiang, Y. Yuan, H. Wang *et al.*, “Sapien: A simulated part-based interactive environment,” in *Proceedings of the IEEE/CVF conference on computer vision and pattern recognition*, 2020, pp. 11 097–11 107.
- [194] L. Liu, W. Xu, H. Fu, S. Qian, Q. Yu, Y. Han, and C. Lu, “Akb-48: A real-world articulated object knowledge base,” in *Proceedings of the IEEE/CVF Conference on Computer Vision and Pattern Recognition*, 2022, pp. 14 809–14 818.
- [195] H. Jiang, Y. Mao, M. Savva, and A. X. Chang, “Opd: Single-view 3d openable part detection,” in *European Conference on Computer Vision*. Springer, 2022, pp. 410–426.
- [196] Y. Mao, Y. Zhang, H. Jiang, A. Chang, and M. Savva, “Multiscan: Scalable rgbd scanning for 3d environments with articulated objects,” *Advances in neural information processing systems*, vol. 35, pp. 9058–9071, 2022.
- [197] H. Geng, H. Xu, C. Zhao, C. Xu, L. Yi, S. Huang, and H. Wang, “Gapartnet: Cross-category domain-generalizable object perception and manipulation via generalizable and actionable parts,” in *Proceedings of the IEEE/CVF Conference on Computer Vision and Pattern Recognition*, 2023, pp. 7081–7091.
- [198] D. Iliash, H. Jiang, Y. Zhang, M. Savva, and A. X. Chang, “S2o: Static to openable enhancement for articulated 3d objects,” *arXiv preprint arXiv:2409.18896*, 2024.
- [199] N. Heppert, M. Z. Irshad, S. Zakharov, K. Liu, R. A. Ambrus, J. Bohg, A. Valada, and T. Kollar, “Carto: Category and joint agnostic reconstruction of articulated objects,” in *Proceedings of the IEEE/CVF Conference on Computer Vision and Pattern Recognition*, 2023, pp. 21 201–21 210.
- [200] J. Guo, Y. Xin, G. Liu, K. Xu, L. Liu, and R. Hu, “Articulatedgds: Self-supervised digital twin modeling of articulated objects using 3d gaussian splatting,” *arXiv preprint arXiv:2503.08135*, 2025.
- [201] J. Kerr, C. M. Kim, M. Wu, B. Yi, Q. Wang, K. Goldberg, and A. Kanazawa, “Robot see robot do: Imitating articulated object manipulation with monocular 4d reconstruction,” *arXiv preprint arXiv:2409.18121*, 2024.
- [202] J. Mu, W. Qiu, A. Kortylewski, A. Yuille, N. Vasconcelos, and X. Wang, “A-sdf: Learning disentangled signed distance functions for articulated shape representation,” in *Proceedings of the IEEE/CVF International Conference on Computer Vision*, 2021, pp. 13 001–13 011.
- [203] F. Wei, R. Chabra, L. Ma, C. Lassner, M. Zollhöfer, S. Rusinkiewicz, C. Sweeney, R. Newcombe, and M. Slavcheva, “Self-supervised neural articulated shape and appearance models,” in *Proceedings of the IEEE/CVF Conference on Computer Vision and Pattern Recognition*, 2022, pp. 15 816–15 826.
- [204] C. Song, J. Wei, C. S. Foo, G. Lin, and F. Liu, “Reacto: Reconstructing articulated objects from a single video,” in *Proceedings of the IEEE/CVF Conference on Computer Vision and Pattern Recognition*, 2024, pp. 5384–5395.
- [205] A. Swaminathan, A. Gupta, K. Gupta, S. R. Maiya, V. Agarwal, and A. Shrivastava, “Leia: Latent view-invariant embeddings for implicit 3d articulation,” in *European Conference on Computer Vision*. Springer, 2024, pp. 210–227.
- [206] W.-C. Tseng, H.-J. Liao, L. Yen-Chen, and M. Sun, “Cla-nerf: Category-level articulated neural radiance field,” in *2022 International Conference on Robotics and Automation (ICRA)*. IEEE, 2022, pp. 8454–8460.
- [207] Z. Jiang, C.-C. Hsu, and Y. Zhu, “Ditto: Building digital twins of articulated objects from interaction,” in *Proceedings of the IEEE/CVF Conference on Computer Vision and Pattern Recognition*, 2022, pp. 5616–5626.
- [208] J. Liu, A. Mahdavi-Amiri, and M. Savva, “Paris: Part-level reconstruction and motion analysis for articulated objects,” in *Proceedings of the IEEE/CVF International Conference on Computer Vision*, 2023, pp. 352–363.
- [209] Y. Weng, B. Wen, J. Tremblay, V. Blukis, D. Fox, L. Guibas, and S. Birchfield, “Neural implicit representation for building digital twins of unknown articulated objects,” in *Proceedings of the IEEE/CVF Conference on Computer Vision and Pattern Recognition*, 2024, pp. 3141–3150.
- [210] Z. Mandi, Y. Weng, D. Bauer, and S. Song, “Real2code: Reconstruct articulated objects via code generation,” *arXiv preprint arXiv:2406.08474*, 2024.
- [211] J. Lei, C. Deng, B. Shen, L. Guibas, and K. Daniilidis, “Nap: Neural 3d articulation prior,” *arXiv preprint arXiv:2305.16315*, 2023.
- [212] J. Liu, H. I. I. Tam, A. Mahdavi-Amiri, and M. Savva, “Cage: controllable articulation generation,” in *Proceedings of the IEEE/CVF Conference on Computer Vision and Pattern Recognition*, 2024, pp. 17 880–17 889.
- [213] J. Su, Y. Feng, Z. Li, J. Song, Y. He, B. Ren, and B. Xu, “Artformer: Controllable generation of diverse 3d articulated objects,” *arXiv preprint arXiv:2412.07237*, 2024.
- [214] L. Le, J. Xie, W. Liang, H.-J. Wang, Y. Yang, Y. J. Ma, K. Vedder, A. Krishna, D. Jayaraman, and E. Eaton, “Articulate-anything: Automatic modeling of articulated objects via a vision-language foundation model,” *arXiv preprint arXiv:2410.13882*, 2024.
- [215] M. Kaup, C. Wolff, H. Hwang, J. Mayer, and E. Bruni, “A review of nine physics engines for reinforcement learning research,” *arXiv preprint arXiv:2407.08590*, 2024.
- [216] E. Todorov, T. Erez, and Y. Tassa, “Mujoco: A physics engine for model-based control,” in *2012 IEEE/RSJ International Conference on Intelligent Robots and Systems*, 2012, pp. 5026–5033.
- [217] N. Koenig and A. Howard, “Design and use paradigms for gazebo, an open-source multi-robot simulator,” in *2004 IEEE/RSJ International Conference on Intelligent Robots and Systems (IROS) (IEEE Cat. No.04CH37566)*, vol. 3, 2004, pp. 2149–2154 vol.3.
- [218] E. Coumans and Y. Bai, “Pybullet, a python module

- for physics simulation for games, robotics and machine learning,” <http://pybullet.org>, 2016–2021.
- [219] O. Michel, “Webots: Professional mobile robot simulation,” *Journal of Advanced Robotics Systems*, vol. 1, no. 1, pp. 39–42, 2004. [Online]. Available: <http://www.ars-journal.com/International-Journal-of-Advanced-Robotic-Systems/Volume-1/39-42.pdf>
- [220] C. D. Freeman, E. Frey, A. Raichuk, S. Girgin, I. Mordatch, and O. Bachem, “Brax - a differentiable physics engine for large scale rigid body simulation,” 2021. [Online]. Available: <http://github.com/google/brax>
- [221] F. Faure, C. Duriez, H. Delingette, J. Allard, B. Gilles, S. Marchesseau, H. Talbot, H. Courtecuisse, G. Bousquet, I. Peterlík, and S. Cotin, “Sofa, a multi-model framework for interactive physical simulation,” 2011. [Online]. Available: <https://api.semanticscholar.org/CorpusID:62022467>
- [222] M. Haiderbhai and L. A. Kahrs, “Simulating surgical robot cutting of thin deformable materials using a rope grid structure,” *IEEE Transactions on Medical Robotics and Bionics*, 2024.
- [223] C. Agabiti, E. Ménager, and E. Falotico, “Whole-arm grasping strategy for soft arms to capture space debris,” in *2023 IEEE International Conference on Soft Robotics (RoboSoft)*. IEEE, 2023, pp. 1–6.
- [224] L. Fang, R. Zhang, C. Vanden Heuvel, R. Serban, and D. Negrut, “Chrono::gpu: An open-source simulation package for granular dynamics using the discrete element method,” *Processes*, vol. 9, no. 10, 2021. [Online]. Available: <https://www.mdpi.com/2227-9717/9/10/1813>
- [225] J. Liang, V. Makoviychuk, A. Handa, N. Chentanez, M. Macklin, and D. Fox, “Gpu-accelerated robotic simulation for distributed reinforcement learning,” in *Conference on Robot Learning*. PMLR, 2018, pp. 270–282.
- [226] J. K. Haas, “A history of the unity game engine,” 2014.
- [227] B. O. Community, *Blender - a 3D modelling and rendering package*, Blender Foundation, Stichting Blender Foundation, Amsterdam, 2018. [Online]. Available: <http://www.blender.org>
- [228] A. Dosovitskiy, G. Ros, F. Codevilla, A. Lopez, and V. Koltun, “CARLA: An open urban driving simulator,” in *Proceedings of the 1st Annual Conference on Robot Learning*, 2017, pp. 1–16.
- [229] M. Neumann, A. Haidu, and M. Beetz, “Urobosim — a simulation-based predictive modelling engine for cognition-enabled robot manipulation,” in *2nd Embodied AI Workshop (CVPR)*, 2021. [Online]. Available: <https://embodied-ai.org/papers/URoboSim.pdf>
- [230] P. Mania, S. Stelzer, G. Kazhoyan, and M. Beetz, “An open and flexible robot perception framework for mobile manipulation tasks,” in *2024 IEEE International Conference on Robotics and Automation (ICRA)*, 2024, pp. 17 445–17 451.
- [231] G. Authors, “Genesis: A universal and generative physics engine for robotics and beyond,” December 2024. [Online]. Available: <https://github.com/Genesis-Embodied-AI/Genesis>
- [232] M. Ivanou, S. Mikhel, and S. Savin, “Robot description formats and approaches,” in *2021 International Conference Nonlinearity, Information and Robotics (NIR)*. IEEE, 2021, pp. 1–5.
- [233] D. Tola and P. Corke, “Understanding urdf: A dataset and analysis,” *IEEE Robotics and Automation Letters*, 2024.
- [234] G. Elkoura, S. Grassia, S. Boonyatera, A. Mohr, P. Jeremias-Vila, and M. Kuruc, “A deep dive into universal scene description and hydra,” in *ACM SIGGRAPH 2019 Courses*. ACM, 2019, pp. 1–48.
- [235] G. H. Nguyen, D. Beßler, S. Stelzer, M. Pomarlan, and M. Beetz, “Translating universal scene descriptions into knowledge graphs for robotic environment,” in *2024 IEEE International Conference on Robotics and Automation (ICRA)*. IEEE, 2024, pp. 9389–9395.
- [236] A.-M. Halacheva, Y. Miao, J.-N. Zaech, X. Wang, L. Van Gool, and D. P. Paudel, “Holistic understanding of 3d scenes as universal scene description,” *arXiv preprint arXiv:2412.01398*, 2024.
- [237] M. S. Hossain, M. R. Ahmed, L. Pullum, S. Jha, and R. Ewetz, “Neuro-symbolic representations of 3d scenes using universal scene description language,” in *Neuro-Symbolic Learning and Reasoning in the era of Large Language Models*, 2023.
- [238] R. Tedrake and the Drake Development Team, “Drake: Model-based design and verification for robotics,” 2019.
- [239] H. Smith, “The metaverse-industrial complex,” *Information, Communication & Society*, pp. 1–18, 2024.
- [240] F. Santucci, F. Frenguelli, A. De Angelis, I. Cuccaro, D. Perri, and M. Simonetti, “An immersive open source environment using godot,” in *Computational Science and Its Applications—ICCSA 2020: 20th International Conference, Cagliari, Italy, July 1–4, 2020, Proceedings, Part VII 20*. Springer, 2020, pp. 784–798.
- [241] S. Brooks, “Markov chain monte carlo method and its application,” *Journal of the royal statistical society: series D (the Statistician)*, vol. 47, no. 1, pp. 69–100, 1998.
- [242] J. Wu, I. Yildirim, J. J. Lim, B. Freeman, and J. Tenenbaum, “Galileo: Perceiving physical object properties by integrating a physics engine with deep learning,” *Advances in neural information processing systems*, vol. 28, 2015.
- [243] M. Link, M. Schwarz, and S. Behnke, “Predicting physical object properties from video,” in *2022 International Joint Conference on Neural Networks (IJCNN)*. IEEE, 2022, pp. 1–7.
- [244] M. Mao, H. Va, and M. Hong, “Video classification of cloth simulations: Deep learning and position-based dynamics for stiffness prediction,” *Sensors*, vol. 24, no. 2, p. 549, 2024.
- [245] B. Koonce, “Resnet 50,” in *Convolutional neural networks with swift for tensorflow: image recognition and dataset categorization*. Springer, 2021, pp. 63–72.

- [246] K. Simonyan and A. Zisserman, “Very deep convolutional networks for large-scale image recognition,” *arXiv preprint arXiv:1409.1556*, 2014.
- [247] K. L. Bouman, B. Xiao, P. Battaglia, and W. T. Freeman, “Estimating the material properties of fabric from video,” in *Proceedings of the IEEE international conference on computer vision*, 2013, pp. 1984–1991.
- [248] M. Walker, G. Pizzuto, H. Fakhruddin, and A. I. Cooper, “Go with the flow: deep learning methods for autonomous viscosity estimations,” *Digital discovery*, vol. 2, no. 5, pp. 1540–1547, 2023.
- [249] T. Xie, Z. Zong, Y. Qiu, X. Li, Y. Feng, Y. Yang, and C. Jiang, “Physgaussian: Physics-integrated 3d gaussians for generative dynamics,” in *Proceedings of the IEEE/CVF Conference on Computer Vision and Pattern Recognition*, 2024, pp. 4389–4398.
- [250] J. Straub, T. Whelan, L. Ma, Y. Chen, E. Wijmans, S. Green, J. J. Engel, R. Mur-Artal, C. Ren, S. Verma, A. Clarkson, M. Yan, B. Budge, Y. Yan, X. Pan, J. Yon, Y. Zou, K. Leon, N. Carter, J. Briales, T. Gillingham, E. Mueggler, L. Pesqueira, M. Savva, D. Batra, H. M. Strasdat, R. D. Nardi, M. Goesele, S. Lovegrove, and R. Newcombe, “The replica dataset: A digital replica of indoor spaces,” 2019. [Online]. Available: <https://arxiv.org/abs/1906.05797>
- [251] A. Szot, A. Clegg, E. Undersander, E. Wijmans, Y. Zhao, J. Turner, N. Maestre, M. Mukadam, D. Chaplot, O. Maksymets, A. Gokaslan, V. Vondrus, S. Dharur, F. Meier, W. Galuba, A. Chang, Z. Kira, V. Koltun, J. Malik, M. Savva, and D. Batra, “Habitat 2.0: Training home assistants to rearrange their habitat,” in *Advances in Neural Information Processing Systems (NeurIPS)*, 2021.
- [252] A. Chang, A. Dai, T. Funkhouser, M. Halber, M. Nießner, M. Savva, S. Song, A. Zeng, and Y. Zhang, “Matterport3d: Learning from rgb-d data in indoor environments,” 2017. [Online]. Available: <https://arxiv.org/abs/1709.06158>
- [253] M. Khanna*, Y. Mao*, H. Jiang, S. Haresh, B. Shacklett, D. Batra, A. Clegg, E. Undersander, A. X. Chang, and M. Savva, “Habitat Synthetic Scenes Dataset (HSSD-200): An Analysis of 3D Scene Scale and Realism Tradeoffs for ObjectGoal Navigation,” *arXiv preprint*, 2023.
- [254] E. Kolve, R. Mottaghi, W. Han, E. VanderBilt, L. Weihs, A. Herrasti, M. Deitke, K. Ehsani, D. Gordon, Y. Zhu, A. Kembhavi, A. Gupta, and A. Farhadi, “Ai2-thor: An interactive 3d environment for visual ai,” 2022. [Online]. Available: <https://arxiv.org/abs/1712.05474>
- [255] M. Deitke, E. VanderBilt, A. Herrasti, L. Weihs, J. Salvador, K. Ehsani, W. Han, E. Kolve, A. Farhadi, A. Kembhavi, and R. Mottaghi, “Proctor: Large-scale embodied ai using procedural generation,” 2022. [Online]. Available: <https://arxiv.org/abs/2206.06994>
- [256] F. Xia, A. R. Zamir, Z. He, A. Sax, J. Malik, and S. Savarese, “Gibson Env: real-world perception for embodied agents,” in *Computer Vision and Pattern Recognition (CVPR), 2018 IEEE Conference on*. IEEE, 2018.
- [257] H. Fu, B. Cai, L. Gao, L.-X. Zhang, J. Wang, C. Li, Q. Zeng, C. Sun, R. Jia, B. Zhao *et al.*, “3d-front: 3d furnished rooms with layouts and semantics,” in *Proceedings of the IEEE/CVF International Conference on Computer Vision*, 2021, pp. 10933–10942.
- [258] C. Yeshwanth, Y.-C. Liu, M. Nießner, and A. Dai, “Scannet++: A high-fidelity dataset of 3d indoor scenes,” in *Proceedings of the International Conference on Computer Vision (ICCV)*, 2023.